Sustainable
Energy & Fuels

ROYAL SOCIETY
OF CHEMISTRY

REVIEW

View Article Online
View Journal | View Issue

Check for updates

Cite this: *Sustainable Energy Fuels*, 2024, **8**, 3476

Published on 27 2024. Downloaded by Fail Open on 23.07.2025 10:35:13.

Flatland materials for photochemical and electrochemical nitrogen fixation applications: from lab-door experiments to large-scale applicability

Syed Asim Ali, Iqra Sadiq and Tokeer Ahmad *

Received 28th April 2024
Accepted 26th June 2024

DOI: 10.1039/d4se00565a

rsc.li/sustainable-energy

Rational design of materials in a catalytic system is the main determinant of the efficiency of sustainable energy sources. Significant efforts have focused on the study and development of flatland two-dimensional (2D) materials (MXenes, MBenes, transition metal dichalcogenides/phosphides (TMDs/TMPs), phosphorene, graphene derivatives) towards energy-driven aspirations in consideration of their superior physiochemical properties as compared to their non-layered counterpart materials, surpassing their transport properties and conductivity. Herein, we aim to provide a detailed account of where the flatland materials currently stand to achieve the goal of sustainability in light of their photochemical and electrochemical nitrogen fixation applications. As of now, numerous challenges have limited the expansion of 2D-material derived nitrogen fixation operations for scalable applications. Therefore, we summarized techno-economic analysis and future perspectives of nitrogen fixation applications in relation to their practical ammonia applicability. We have briefly summarized the functionality of flatland materials and classified them on the basis of their photochemical and electrochemical efficiencies.

Introduction

The present era of energy utilization has predominantly involved the extensive use of fossil-derived fuels dating back to the dawn of the industrial revolution. The last century paved the way for oil reserves, consolidating the fossils in strengthening economies across the globe.[1,2] In the face of environmental challenges and the urgency to mitigate the effects of global warming, the pursuit of sustainable energy has emerged as a global imperative. Sustainable adaptability can be achieved by subscribing to those energy sources and maneuvers that meet the world's present needs and do not obstruct the scope of future generations for utilizing natural resources. Renewable energy resources such as hydrogen production *via* overall water splitting and hydrocarbon fuels originating from CO_2 reduction

---

Nanochemistry Laboratory, Department of Chemistry, Jamia Millia Islamia, New Delhi-110025, India. E-mail: tahmad3@jmi.ac.in; Tel: +91-11-26981717, ext. 3261

Syed Asim Ali

Syed Asim Ali completed his undergraduate and post-graduate studies at Jamia Millia Islamia, New Delhi. Subsequently, he joined the Nanochemistry Lab under the supervision of Prof. Tokeer Ahmad. His research interests include the design of nano-catalysts, energy conversion and sensing applications, computational chemistry and techno-economic analysis. He is currently working on the synthesis and characterization of molybdenum chalcogenides-based heterojunctions for their multi-functional applications.

Iqra Sadiq

Iqra Sadiq graduated from K. R. Mangalam University and completed her post-graduate studies at G. D. Goenka University, Gurugram. She then joined Jamia Millia Islamia University, New Delhi, as a research scholar under the supervision of Prof. Tokeer Ahmad, and is currently working on the chemical synthesis and structural characterization of some functional nanostructures for environmental remediation and energy-based applications.

This journal is © The Royal Society of Chemistry 2024

Published on 27 2024. Downloaded by Fail Open on 23.07.2025 10:35:13.

reaction (CO_2RR) are the front-runners aimed at alleviating carbon emissions and promoting a transition to a low-carbon economy.[3–5] Despite significant progress in the research of hydrogen evolution reaction (HER) and CO_2RR, both these processes have some disadvantages[6] such as extraordinary costs associated with storage and transportation of the hydrogen carrier and separation of the desired product from the mixture of carbon-based products. Utilizing ammonia (NH_3) as the source of renewable energy and as the transport medium for carrying H_2 fuel comes with several benefits such as its compactness and higher efficiency in durable and longer distance energy endeavours.[7,8] The market size of NH_3 is expanding dramatically, which is substantially driven by its conventional use in agricultural and manufacturing sectors alongside its growing interest as a carbon-neutral energy carrier. Among the different routes of NH_3 synthesis, one natural enzymatic reduction phenomenon is the conversion of nitrogen (N_2) *via* nitrogenase that replenishes the N-cycle.[9–11] Nevertheless, the lethargic kinetics of NH_3 formation restrict the applicability of this pathway. Production of NH_3 from photochemical and electrochemical N_2 fixation processes at ambient conditions is an emerging area of research that has gained attention on account of the industrial significance of NH_3 as the precursor to manufacturing many important chemicals and fertilizers.[12–15] The efficiency of the photochemical and electrochemical nitrogen reduction reaction (NRR) for NH_3 production relies upon the prudent choice of a catalytic system that can accelerate the reaction dynamics.[16–21] A wide array of catalytic systems has been constructed by researchers to augment the yield of the targeted renewable energy carrier during energy-conversion applications. These systems include perovskites,[22,23] mesoporous materials,[24,25] transition metal oxides[26]/phosphides[27]/dichalchogenides[28]/carbonitrides/borides,[29,30] single-atom catalysts (SACs),[31,32] layered double hydroxides (LDHs),[33,34] and carbon-based derivatives.[35]

Tokeer Ahmad

Prof. Tokeer Ahmad (graduated from IIT Delhi) is the full Professor of Chemistry at JMI Delhi. Prof. Ahmad has supervised 16 PhD's, 79 postgraduates, 10 projects, and published 194 research papers, one patent and three books with research citation of 7610, h-index of 52 and i10-index of 153. Prof. Ahmad is the recipient of the CRSI Medal, MRSI Medal, SMC Bronze Medal, ISCAS Medal, Inspired Teacher's President of India Award, DST-DFG award, Distinguished Scientist Award, Maulana Abul Kalam Azad Excellence Award of Education, Teacher's Excellence Award, and was elected as Member of the National Academy of Sciences, India. Prof. Ahmad is also an admitted Fellow of the Royal Society of Chemistry (FRSC), UK.

Among these materials, the development of flatland materials has been a ground-breaking achievement in materials science and nanotechnology,[36] offering unique properties and potential applications across interdisciplinary fields,[37] including electronics,[38] energy storage,[39] catalysis,[40] and biomedicine.[41] In addition, the recent advances in flatland materials have ascertained their energy conversion applications.[42] Chemical strategies, such as doping,[43] surface modification,[44] and heterostructure engineering,[45] have been employed for tuning and engineering the properties of flatland materials for energy conversion applications. The functionalization and integration into a heterojunction formation have led to the development of novel devices with enhanced performance and functionality.[46] The rise of graphene/graphitic nitride derivatives paved the doors of 2D compounds, as these materials possess remarkably higher surface area and tunable electronic properties that are highly sought after for catalytic transformations.[47,48] As of now, different flatland materials have been designed and exploited in energy conversion applications, *viz.*, hydrogen and oxygen evolution reactions (HER/OER)[28,35] and CO_2 sequestration.[49] Nevertheless, the research of these layered materials toward NRR is still at its nascent stage, and researchers are showing immense interest in their applicability as state-of-art catalytic systems for the NRR process. Noteworthily, the origin of the catalytic excellence of several 2D materials is linked to their exposed edge facets and defect surfaces that also govern their NRR performance.[49,50] Diverse modification attempts have been made by researchers to augment the catalytic efficiency of flatland materials, such as surface functionalization,[51] intercalation,[52] and incorporating porous materials or non-layered materials (such as porous organic polymers (POPs) or TiO_2) to develop heterojunctions.[28,53,54] These chemical strategies to tailor the physicochemical properties of flatland materials require optimized reaction conditions at the time of synthesis, such as the solvent selectivity, thermal conditions and exfoliating parameters, to extract monolayers of 2D materials.[48] To achieve a higher yield during the NRR process, the enhancement of exposed surface sites is the primary factor. The ideal flatland material-based catalytic system is expected to provide an inherent basal plane activation, while possessing higher selectivity for N_2-adsorption as compared to H-adsorption as an HER, making it a thermodynamically more viable process than NRR. The efficient synergetic relationship between the catalytic activity and long-term stability of 2D materials-based catalysts is necessary to have robustness during the NRR process. The stability and durability of flatland materials suffer from several bottlenecks, which restrict their performance. The 2D materials usually comprise defects, such as vacancies, grain boundaries, and edge irregularities, which ideally serve as active sites. However, they can also be prone to degradation, leading to the loss of catalytic activity. The 2D materials can undergo unwanted oxidation or reduction reactions, especially under extreme pH conditions or at high temperatures, which can alter their electronic structure and catalytic properties. When 2D materials are exploited during heterojunctions formation, weak interactions between the 2D material and the support can lead to detachment and

Published on 27 2024. Downloaded by Fail Open on 23.07.2025 10:35:13.

loss of the active material. Fabricating 2D materials with consistent quality and physicochemical properties on a large scale is challenging. Variations in synthesis methods can lead to inconsistencies in the catalyst performance. Addressing these challenges involves synthetic advancements, enhancing the understanding of the material properties under operational conditions, and developing strategies to protect and stabilize 2D materials during catalytic transformations.

Synthetic advancements in the development of flatland materials

For the systematic exploitation of 2D materials to the maximum extent, the prudent choice of the synthetic protocol is necessary. Improved synthesis techniques lead to higher-quality 2D materials with tailored properties, addressing many of the challenges associated with their stability and durability. There are plenty of top-down and bottom-approaches that have been reported in the literature for the fabrication of functional and advanced materials, such as the facile hydrothermal route, sol–gel/polymeric citrate precursor method, reverse micellar, chemical vapor deposition, mechanical/chemical exfoliation, lithography techniques and many more.[55–60] One of the most important routes of constructing MXene and MBene is their etching from the parental MAX/MAB phases, where A is basically the transition metal (such as Al, Ga or Sn). The MAX/MAB phase precursors are generally prepared *via* powder metallurgy techniques, followed by etching using stronger acid etchants such as HF/H_2SO_4 to selectively eliminate the A-layers. The etching routes expose the MXene/MBene layers, which are then washed and delaminated to obtain colloidal suspensions or films of MXene/MBene nanosheets.[61] Exfoliation of bulk MXene/MBene materials involve breaking down the layered bulk MXene/MBene into individual nanosheets, which can then be dispersed in solvents to obtain colloidal suspensions or thin films.[62,63] Another interesting method of designing MXenes and MBenes is the intercalation/delamination method, in which the concerned-intercalated precursors are subjected to chemical or electrochemical treatments to selectively eject the interlayer ions or nanoparticles, leading to the delamination of the layered structure into MXene/MBene nanosheets.[64] Alongside these exfoliation and top-down methodologies, there is the growing interest of researchers toward designing MXenes and MBenes through bottom-up approaches, such as chemical vapor deposition (CVD)[65] and facile hydrothermal method,[66] without utilizing environmentally hazardous F-based etchants that are not economical for the scalable synthesis of MXene/MBene nanosheets.[67] These methodologies offer versatile chemical strategies for developing MXene/MBene materials with tailored properties and structures to ensure their simplified integration into various energy-related applications. Recent attempts have focused on optimizing the synthesis parameters, scaling up the production and exploring novel MXene/MBene catalysts to expand their range of applications.[68,69] For the development of TMDs, there are diverse fabrication routes that ensure morphological and structural tailoring to a larger extent, such as CVD, template-assisted synthesis, mechanical/chemical/liquid-phase exfoliation. CVD provides a simplified protocol to prepare high-quality TMDs nanosheets with higher specific surface areas.[70] By tuning different reaction parameters like the temperature, pressure, precursor concentration, and substrate type, the rate of nucleation and growth can be modulated to design the desired morphology of TMDs materials required for targeted applications. Exfoliation techniques of synthesizing TMDs generally involve manually peeling off thin layers of bulk TMDs to acquire TMDs monolayers with great control over the thickness of the nanosheets. The facile hydrothermal route ensures the construction of TMDs having controlled size and desirable morphological and structural properties under 180–200 °C temperature range at higher pressure.[26,28] These routes have been comprehensively discussed in reviews elsewhere.[70] The fabrication routes of TMPs generally encompass different methods based on the precursors of P, such as elemental phosphorus, phosphorenes or organic phosphines. To achieve morphological tunability and higher specific surface area, P-pyrolysis with a C-based compound is an excellent method that hampers the aggregation of TMP nanosheets and improves its electrical conductance. Just like other 2D materials, there are different routes of TMPs fabrication, such as phosphorizing metal sources,[71,72] CVD, solid state method, and hydrothermal synthesis, as detailed in reviews elsewhere.[27] The fabrication routes of carbon-based derivatives are more or less similar to those of other 2D materials, such as CVD, exfoliation techniques for $g\text{-}C_3N_4$,[73] and the Hummer's method for synthesizing graphene oxide (GO) and reduced-GO. These fabrication routes all fundamentally involve the utilization of different chemical reducing agents, such as hydrazine, hydroiodic acid, or thermal treatment under reducing atmospheres.[47] Despite the success of these methods in designing flatland materials, the achievement of scalability in their synthesis is fundamental for realizing their industrial applications. State-of-art approaches such as high-throughput screening techniques can be exploited, which involve systematically screening a large number of reaction conditions and parameters to identify optimal conditions for the preparation of 2D materials.[74] Reaction variables like the reactant concentrations, reaction temperatures, mixing rates, and reactor geometry can be optimized to attain an equilibrium between the maximized yield and minimized production costs.[75–77] Pilot-scale operations and process modelling can be utilized to determine the critical factors affecting scalability and guide the design of large-scale 2D materials synthesis processes. The advancements in the fabrication routes are pivotal for the construction and application of 2D materials in NRR.

Nitrogen fixation

N_2 fixation is regarded as one of the most significant processes to transform atmospheric N_2 into NH_3 and other value-added N-based compounds. This transformation can be achieved through a wide array of pathways, such as the conventional Haber–Bosch method, biological or microorganisms-assisted N_2 fixation. Artificial photochemical N_2 fixation is

Published on 27 2024. Downloaded by Fail Open on 23.07.2025 10:35:13.

a sustainable route for developing nitrogenous compounds by utilizing photon energy and replicating the natural N_2 fixation process. Similarly, electrochemical N_2 fixation also should produce N-based chemical feedstock at the expense of electrical energy.[78–81] Among the various nitrogenous compounds, NH_3 holds relatively superior industrial significance and day-to-day applicability, as it serves as the fundamental precursor in manufacturing several fertilizers and purifiers.[82] Alongside, condensed NH_3 promises applications in the energy conversion on account of its greater gravimetric density and transportability as compared to H_2 fuel. The recent trend of sustainable energy transition suggests an exponential growth in the demand of H_2 fuel by 2050. However, there are challenges in achieving efficient transportation over a larger distance in compact containers. In contrast, NH_3 is relatively easy to transport with the requirement of a less complicated infrastructure.[83,84] Green NH_3 synthesis relies upon the accelerated production of H_2 simultaneously with the extraction of N_2 from the environment *via* air separating techniques. Photochemical and electrochemical NH_3 production routes are carbon-neutral pathways that aspire to generate NH_3 efficiently and economically in the near future.[85,86] NH_3 is most commonly produced commercially *via* Haber–Bosch reactions, which require high temperatures (400–500 °C) and pressure (15–25 MPa). A simpler and environmentally benign protocol of NH_3 is sought after to accelerate the pace of NH_3 usage as an energy carrier.

NRR applications of flatland materials

Flatland materials have garnered significant attention for effective NH_3 production due to their unique physicochemical features. These 2D materials offer a diverse range of properties and structures that can be tailored *via* different compositional and structural modifications, such as surface functionalization, heterostructure engineering, and optimization of electronic and catalytic properties.[87] Perseverant advancements into the rational design, characterizations and applications of 2D materials affirm their scalability in sustainable nitrogen fixation technologies.

Photochemical applications

The reaction mechanism of photochemical NRR generally progresses *via* the formation of several reactive intermediate species like N-based radicals and adsorbed N-intermediates that have to effectively undergo the hydrogenation reaction, followed by desorption to generate NH_3.[88] The excellent optoelectronic and surface properties of 2D materials are of paramount importance in mediating the thermodynamic landscape of NRR by providing the favourable free energies and lower reaction barrier during the surface reactions on the active materials.

MXenes- and MBenes-based photocatalysts

MXenes and MBenes have emerged as two of the latest classes of flatland materials that hold a plethora of potential for heterogeneous catalysis, especially in energy-conversion applications, owing to their enormously higher exposed active sites and unusual layered structures.[89] Current research has hinted that MXenes- and MBenes-based catalytic systems have advanced the enhancement in the rate of N_2-adsorption/activation and its conversion into NH_3 through photochemical and electrochemical NRR processes.[90–92] As of now, the quantum yield of MXenes-led NRR remains lower as compared to the non-sustainable routes of NH_3 synthesis. This is the main reason that a deeper understanding of the mechanism is requisite to optimize the activity of MXenes. Gao *et al.*[93] fabricated a unique MXene-based heterostructured photocatalyst composed of Co-decorated Ti_3C_2/TiO_2 for effective nitrogen fixation. The group demonstrated that the tailoring of the surface activity of N_2 was due to the presence of Co-atoms, as the extent of chemisorption was altered. The optimized photocatalyst achieved as high as 110 μmol g^{-1} h^{-1} NH_4^+ yield in the absence of any sacrificial hole acceptor species. Hao *et al.*[94] hydrothermally constructed a RuO_2-incorporated TiO_2–$Ti_3C_2T_x$ photocatalytic system to examine its nitrogen fixation performance at ambient conditions. The group revealed that the augmented activity of the as-developed catalytic system was due to the symbiotic effects between the MXene/metal oxides, and to the efficient N_2-activation over light exposure. Liao *et al.*[95] showcased the role of Ti_3C_2 in augmenting the NRR activity of the P25 (TiO_2) photocatalyst, attributed to its higher exposed active sites and marvelous electrical conductance. In addition to that, the improved N_2-adsorption over the Ti_3C_2-P25 photocatalyst resulted in its 5-fold higher NRR performance as compared to pristine P25. The close-knit relationship between Ti_3C_2-P25 was realized by X-ray photoelectron spectroscopy (XPS), as illustrated in Fig. 1(a)–(d). The photochemical results inferred enhanced NH_3 selectivity over H_2 evolution on account of the relatively higher chemisorption of N_2 over the H-atoms. Furthermore, the lower conduction band position of Ti_3C_2 also favoured the NRR, as can be seen in Fig. 1(e). Shen *et al.*[96] engineered a ligand-bridged $Ti_3C_2O_x$/MIL-125(Ti)-based MXene/MOF photocatalyst to favourably couple the O-terminal groups (MXene) with the COO-groups (MOF). This type of coordination linkage facilitated the charge migration *via* heterojunction formation during the NRR process. The as-prepared photocatalyst displayed a remarkable NH_3 production rate as high as ~103 μmol g_{cat}^{-1} h^{-1}, which was ascribed to the monodirectional channelization of electron carriers from MOF to MXene. Intermediary species formed during the course of the NRR experiment over the optimized $Ti_3C_2O_x$/MIL-125(Ti) photocatalyst were assessed *via* DRIFTS technique, which proved the N_2-adsorption and activation due to the advent of peaks corresponding to N-based intermediates, as illustrated in Fig. 2(a). These observations indicated the probable symmetric side-on mechanistic route for the NH_3 production. The authors utilized density functional theory (DFT) calculations to investigate the impact of ligand-bridging on the dynamics of N_2-activation. Bader charge analysis and the corresponding 2D curve of the $Ti_3C_2O_x$/MIL-125(Ti) photocatalyst revealed the extensive charge migration occurring through the ligand molecular bridge (LMB). Based on the hydrogenation reaction step of

Published on 27 2024. Downloaded by Fail Open on 23.07.2025 10:35:13.

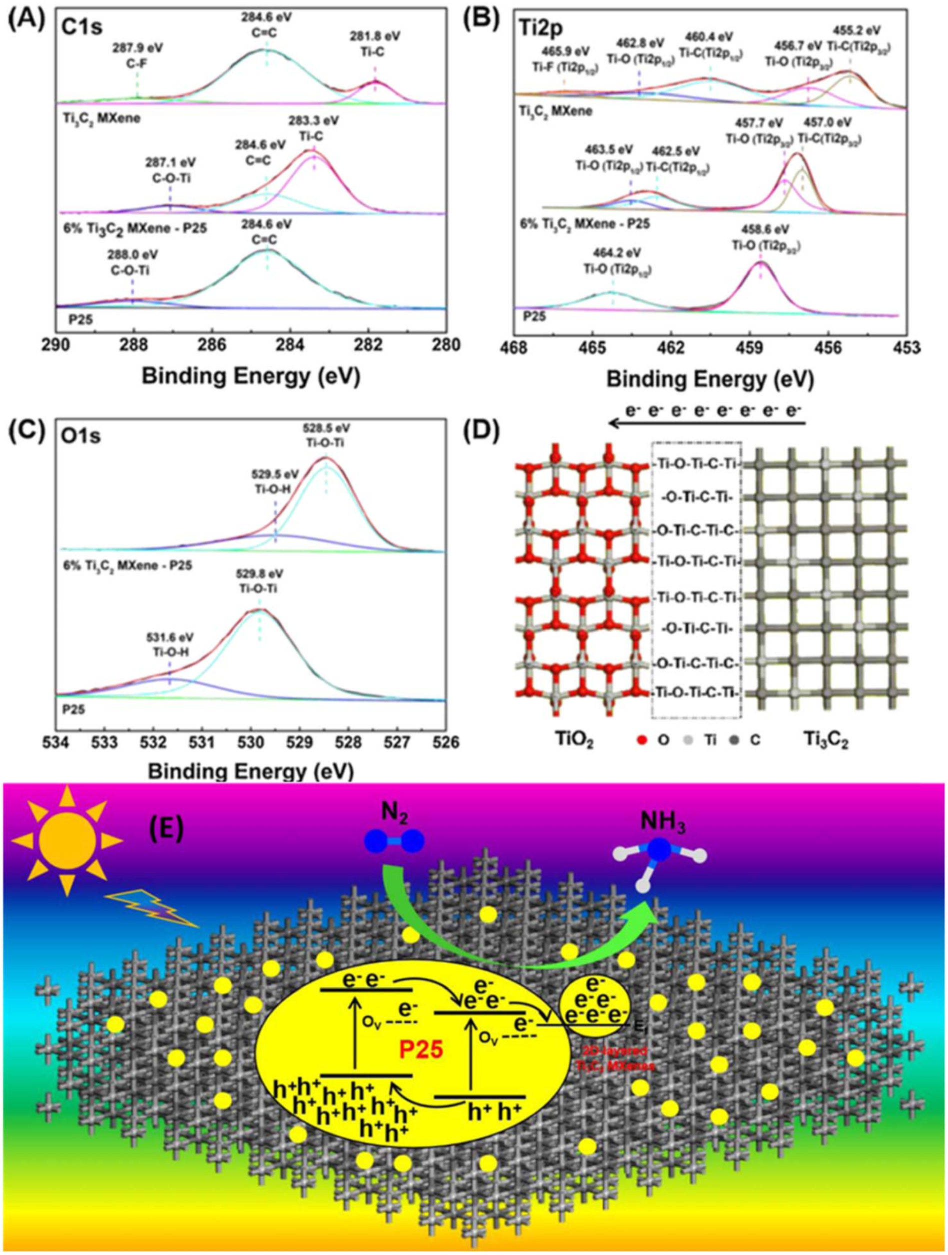

Fig. 1 Core-level spectra of (A) C 1s, (B) Ti 2p, (C) O 1s of bare P25(TiO_2), Ti_3C_2 and the optimized Ti_3C_2-P25 heterostructure. (D) Chemical interactions between TiO_2 and Ti_3C_2. (E) Reaction mechanism of the photochemical NRR for NH_3 formation over the Ti_3C_2-P25 heterostructure. Reproduced with permission.[95] Copyright 2020, Elsevier.

adsorbed-N_2 over $Ti_3C_2O_x$/MIL-125(Ti), NRR could have proceeded *via* two different distal and alternating pathways, as shown in Fig. 2(b). Both reaction mechanisms exhibited varying energy barriers, where the alternating route inferred a relatively lesser uphill energy barrier. In addition, the authors analyzed the modifications in the N–N bond order in the span of the reaction mechanism to further supplement their identification of the probable NRR route. Based on the bond length values of the N–N bonds in both pathways, the pronounced bond elongation in the alternating route provided the evidence that it was the predominant course of NRR. Just like their MXenes counterparts, MBenes have also recently emerged as active materials for the photocatalytic NRR process. Zhang *et al.*[97] developed the unique Ni_3B-incorporated N-vacant g-C_3N_4 (VN-CN) to augment the N_2 fixation efficiency for NH_3 generation. The group ascertained the Schottky junction-formation between MBene and VN-CN, which led to the improved light harvesting and higher exposed sites availability for adsorbing and activating N_2 molecules. The optimized Ni_3B/N-vacant g-C_3N_4 photocatalyst revealed a rate of NH_3 production as high as 7.68 mM g^{-1} h^{-1}, which was nearly 7-fold higher than bare g-C_3N_4. These recent achievements in MXenes and MBenes infer the potential of these 2D-materials toward NRR applications.

Published on 27 2024. Downloaded by Fail Open on 23.07.2025 10:35:13.

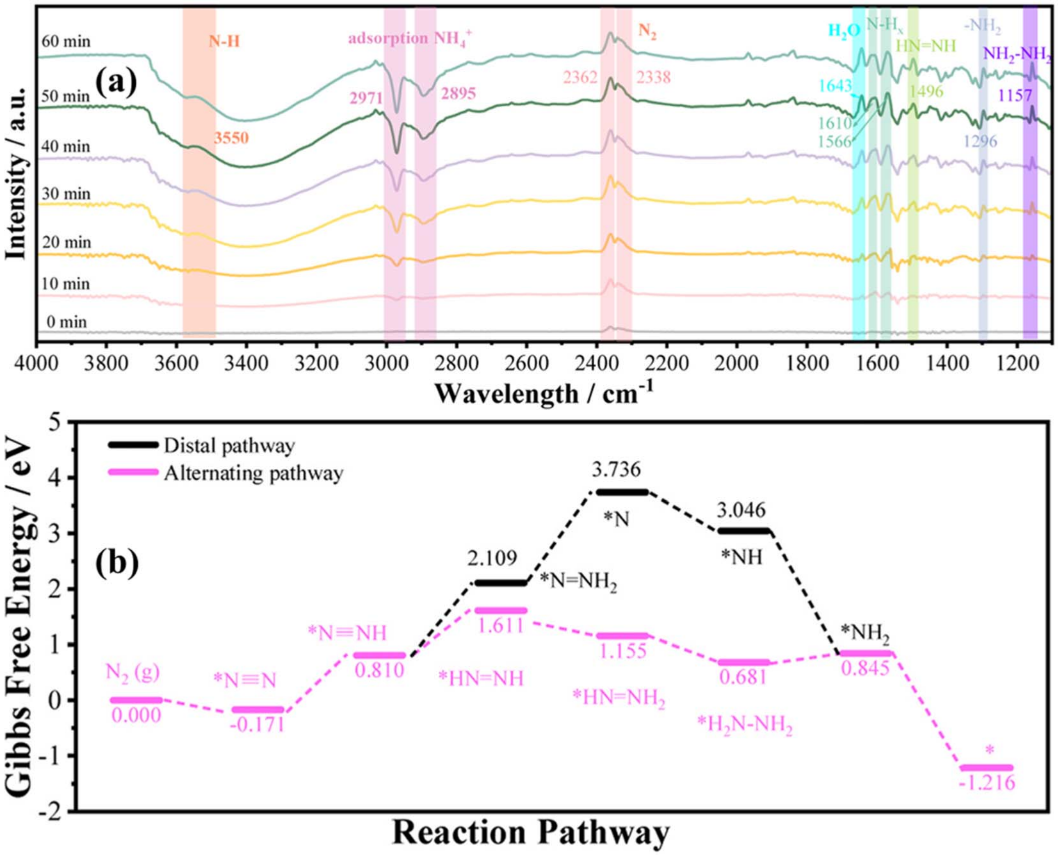

Fig. 2 (a) *In situ* infrared spectra of the optimized $Ti_3C_2O_x$/MIL-125(Ti) heterojunctions analyzed at the time of photochemical NH_3 generation. (b) Thermodynamic landscape for alternating and distal reaction mechanisms over $Ti_3C_2O_x$/MIL-125(Ti). Reproduced with permission.[96] Copyright 2024, Elsevier.

TMDs-based photocatalysts

TMDs have attained significant benchmarks in the field of photochemical NRR on account of their uncommon electronic properties, higher specific surface area, lower band energy and facilitated visible light absorption. TMDs possess active sites with favourable free energies that accelerate the adsorption/activation of nitrogen molecules, leading to efficient NH_3 conversion.[98,99] Alongside their unique physicochemical properties, two important chemical strategies to enhance the NRR activity of TMDs are structural and compositional modifications. The ability of TMDs to accommodate various dopants and functional groups, in addition to their ability to form heterojunctions with other conducting materials, remarkably augment their NRR response. Nevertheless, TMDs suffer from several bottlenecks, such as their limited chemical and thermal stability during photochemical environment, which consequently lead to the oxide formation and photo-corrosiveness of TMD-photocatalysts. Moreover, a profound understanding of the underlying NRR mechanisms is requisite to optimize the catalytic efficiency and stability of TMDs for practical applications. By developing novel TMDs-based heterojunction photocatalysts for energy conversion applications,[26,28] researchers have made satisfactory progress in the past few years, especially for realizing their potential in NRR applications. Recently, Ma *et al.*[100] illustrated the unique interfacial chemical bonding between MoS_2/In-Bi_2MoO_6, which resulted in the enhancement of the NRR performance of the as-developed heterostructured photocatalyst fabricated *via* electrostatic self-assembly route. The group ascertained the advent of the Mo–S intermolecular chemical bonding between the heterostructured photocatalyst to be the primary influencing factor that facilitated the charge-transfer dynamics at the interfacial contact. The theoretical investigations inferred the transfer of electron carriers from MoS_2 to the antibonding orbitals of N_2-molecules for its activation. The optimized MoS_2–In-Bi_2MoO_6 heterostructured photocatalyst exhibited ∼90 μmol g_{cat}^{-1} h^{-1} rate of NH_3 production. Based on the experimental observations, the authors revealed the significant role of MoS_2 in impeding the generation of NO_3^- species, which is an offshoot of the oxidation reaction of the NH_3/NH_4^+ present in the aqueous solution. Therefore, this study clearly depicted the role of the TMDs-based photocatalyst for the selective N_2 photo-reduction reaction. To further highlight the role of MoS_2 in achieving higher photocatalytic NRR performance, Hu *et al.*[101] proposed an excellent study where they regulated the edge sites of MoS_2 to augment the NRR performance. The S-rich edge sites of MoS_2 are relatively exposed active sites that are responsible for the

Published on 27 2024. Downloaded by Fail Open on 23.07.2025 10:35:13.

reduction reaction as compared to the S-atoms present on the basal planes. It was revealed that Mn-doping effectively enhanced the NRR activity of MoS_2 by improving its edges. This led to the modulation of S-edges that facilitated the adsorption of N_2 molecules and lowered the NRR energy barrier. Hydrothermally-derived optimized Mn-doped MoS_2 depicted an NH_3 yield as high as ∼213 μmol g_{cat}^{-1} h^{-1} without using any sacrificial electron donor species, which was found to be nearly 5-fold higher than that for the bare MoS_2 photocatalyst. Recently, Yao *et al.*[102] constructed a TMDs/metal organic framework (MOF) heterostructured photocatalyst composed of WS_2/ZIF-8 to examine its photochemical NRR activity using tap water in real/simulated solar energy. The optimized photocatalyst revealed an NH_3 production rate as high as ∼191.6 μmol g_{cat}^{-1} h^{-1}, as can be seen in Fig. 3(a). The accelerated NRR performance was attributed to the enhanced light harvesting and higher separation of photo-excited charge carriers. In addition, the close-knit interfacial contact between WS_2/ZIF-8 led to the pronounced weakening of the N_2 bond and facilitated its activation dynamics during photochemical NRR. Fig. 3(b and c) demonstrates the Bader charge analysis and photocatalytic NRR mechanism for the generation of NH_3. The transfer of electron-carriers from ZIF-8 to WS_2 led to the facilitated reduction of N_2, which was ascribed to the higher availability of electrons on the conduction band of WS_2. Qin *et al.*[104] explored the reaction mechanism of N_2 adsorption/activation over the hexagonal-triclinic biphasic $Mo_{1-x}W_xS_2$ photocatalyst for advancing the rate of NH_3 production. The optimized $Mo_{1-x}W_xS_2$ photocatalyst exhibited an NH_3 evolution rate of ∼111 μmol g_{cat}^{-1} h^{-1}, which was found to be 3.7- and 3-fold higher than that of bare MoS_2 and WS_2. Experimental investigations manifested the favourable doping of W-atoms, which caused the exploitation of electron density states from the W 5d-orbital for the polarization of the adsorbed-N_2 species. This report highlighted the significance of fabricating intramolecular TMDs to achieve an efficient NRR process. These recent advancements in TMDs-led NRR experiments reveal the scope of MoS_2, $MoSe_2$ and WS_2 in accelerating the NH_3 production efficiency by acting either as an active material or as the cocatalyst in heterostructured materials during photochemical transformations.

TMPs and phosphorene-based photocatalysts

TMPs are an emerging class of 2D materials that offer potential eminence when employed as a photocatalyst during the NRR process on account of their unique physicochemical properties that accelerate the transformation of N_2 into NH_3 under light irradiation. These flatland materials possess an edge over other photocatalysts in terms of their improved activity, selectivity, and stability during photocatalytic transformations.[105,106] The excellent optoelectronic properties of TMPs assist in achieving higher efficiency in photochemical NRR processes, ascribed to the improved light absorption and their layered structure that promote the separation and migration of photo-induced charge carriers during photocatalysis. Alongside, TMPs exhibit exceptional surface properties with mesoporous exposed active sites that favour the adsorption/activation of N_2 molecules during NRR. Recently, researchers have attempted to design the heterostructured photocatalytic systems by exploiting the

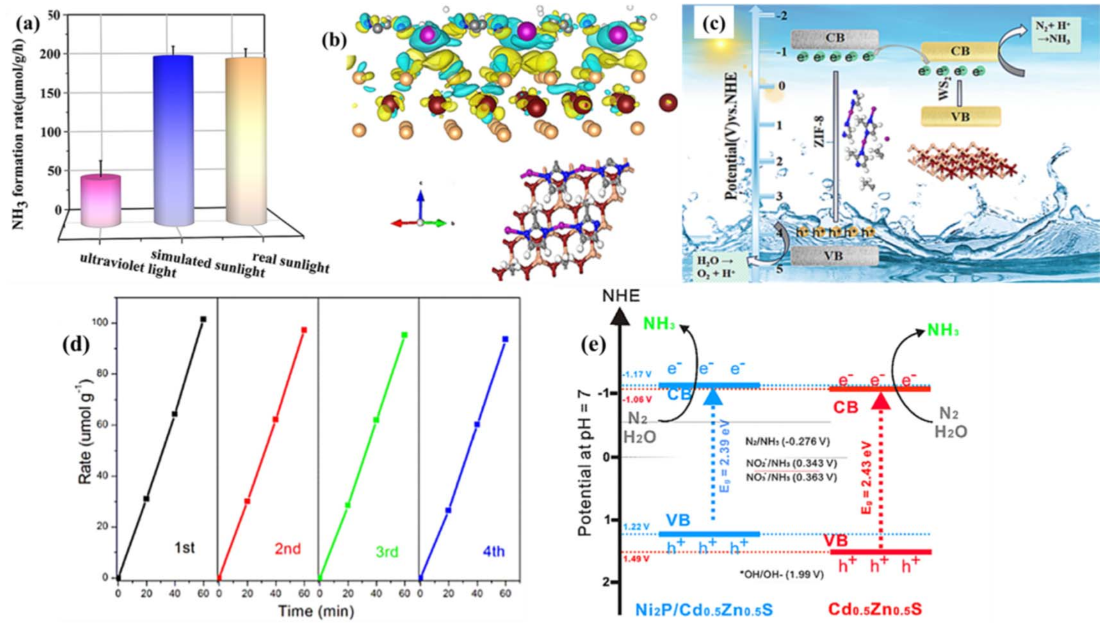

Fig. 3 (a) Photochemical efficiency of the WS_2/ZIF-8 catalytic system towards NRR in varying sources of photon energy. (b) Bader charge analysis and optimized crystal structure of WS_2/ZIF-8. (c) Photochemical NRR mechanism over WS_2/ZIF-8. Reproduced with permission.[102] Copyright 2024, Elsevier. (d) Recyclability test of the optimized $Ni_2P/Cd_{0.5}Zn_{0.5}S$ photocatalyst under visible light irradiation. (e) Photochemical NRR mechanism over $Ni_2P/Cd_{0.5}Zn_{0.5}S$ for NH_3 production. Reproduced with permission.[103] Copyright 2017, Elsevier.

Published on 27 2024. Downloaded by Fail Open on 23.07.2025 10:35:13.

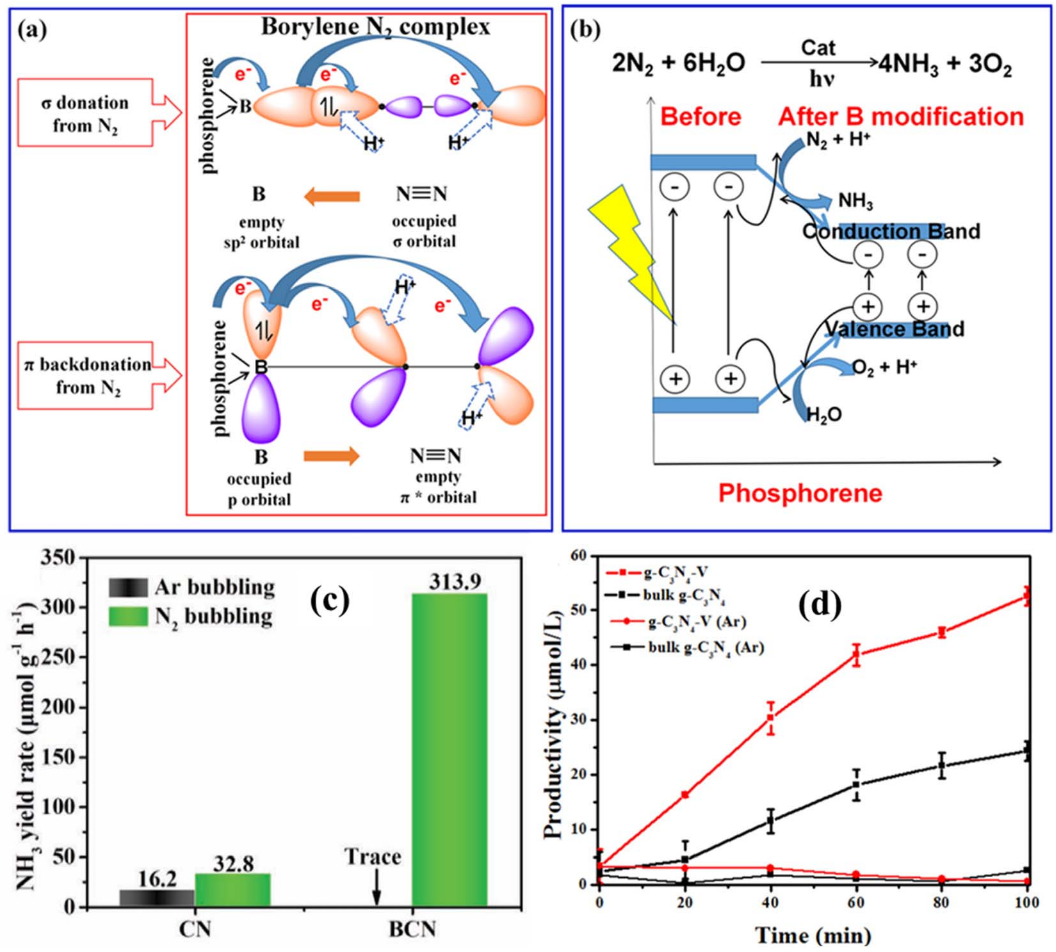

Fig. 4 (a and b) Mechanistic sketch of the photo-reduction of N_2 *via* the B-decorated phosphorene catalyst. Reproduced with permission.[110] Copyright 2021, Elsevier. (c) Photochemical NH_3 production performance of g-C_3N_4 and boron-decorated g-C_3N_4. Reproduced with permission.[111] Copyright 2020, John Wiley and Sons. (d) Photochemical NRR activities of bulk g-C_3N_4 and carbon-vacant g-C_3N_4. Reproduced with permission.[112] Copyright 2019, Elsevier.

remarkable physicochemical properties of TMPs. TMPs exhibit superior stability, robustness and prolonged lifetime during photochemical runs, which particularly make them viable photocatalysts for durable NRR experiments. To demonstrate the higher stability of the TMP-based photocatalysts, Gao *et al.*[107] recently reported on the construction of a g-C_3N_4/Ni_2P/Ni-3D reticulated foam photocatalytic system (CNNPF) for visible light-driven NRR application. The as-designed CNNPF photocatalyst displayed excellent NRR activity as high as ∼373 μmol g_{cat}^{-1} h^{-1} rate owing to the synergetic relationship of g-C_3N_4/Ni_2P, which resulted in the ameliorated charge-transfer dynamics. The group revealed that the 3D-scaffold was responsible for providing the exposed surface-sites availability for N_2 capture. The CNNPF photocatalytic system has shown advanced stability and recyclability after 5 consecutive cycles without significant loss in the activity toward the NRR process. This study demonstrates the significance of designing a stable photocatalytic system for durable NRR application. To highlight the simultaneous HER and NRR applications of TMP-based photocatalysts, Wang *et al.*[108] recently came up with an interesting study where they reported the simple route of designing a unique Ohm–Schottky heterostructured photocatalytic system by utilizing Co–Ni_2P nanosheets. The as-designed modified-CdS/Co–Ni_2P/O-rich Ti_3C_2 photocatalyst revealed a H_2 yield as high as 1.72 mmol h^{-1} and NH_4^+ yield of ∼656.8 μmol L^{-1} h^{-1} with 59.81% AQE. The enhanced HER and NRR performances were ascribed to the improved interfacial charge transfer *via* Ohm–Schottky heterojunctions. Theoretical investigations ascertained the positive impact of decorating the Co–Ni_2P nanosheets over CdS/MXene by providing favourable N_2 adsorption energy and by increasing the conductivity of photocatalyst. Ye *et al.*[103] fabricated a unique $Ni_2P/Cd_{0.5}Zn_{0.5}S$ photocatalyst. The TMP incorporation into $Cd_{0.5}Zn_{0.5}S$ incredibly ameliorated the charge-transfer dynamics during the photochemical NRR process. In the visible-light driven photocatalysis, the NRR activity to achieve NH_3 was found to be ∼101.5 μmol L^{-1} h^{-1} with 4.32% AQE. The heterostructured photocatalyst depicted no loss of activity after four consecutive cycles, as can be seen in Fig. 3(d). Moreover, the advanced performance of the TMP-based $Cd_{0.5}Zn_{0.5}S$ photocatalyst was realized by the modulations of the conduction band (CB) positions after Ni_2P loading, which tuned the photo-reduction

Published on 27 2024. Downloaded by Fail Open on 23.07.2025 10:35:13.

efficiency during NRR, as shown in Fig. 3(e). As compared to $Cd_{0.5}Zn_{0.5}S$, the relatively higher CB position of the heterostructured photocatalyst facilitated the N_2 reduction and lowered the dynamics of oxidation of NH_3 into NO_3^-, which was confirmed by the low yield of the latter (~0.35 μmol L^{-1} h^{-1}). Phosphorene is the P-analog of graphene that is composed of a honeycomb lattice composed of P-atoms. Phosphorene has gained significant research interest owing to its unusual physicochemical properties, such as its higher specific surface area, and its peculiar electronic properties that favour its energy conversion applications.[109] The effectiveness of phosphorene materials in the photochemical NRR application is supported by its recent reports. Wang *et al.*[110] designed the unique non-metallic B-decorated phosphorene (BP) photocatalytic system for investigating its photochemical NRR performance. The group revealed that in the case of P-phosphorene, the adsorption limit of the photocatalyst towards N_2 remains limited. However, the BP-photocatalyst has shown its structural superiority to enhance the rate of N_2 capture by the utilization of vacant and filled sp^2- and p-orbitals, respectively. This ensured the better electron-acceptance and -donation between the σ–π^* orbitals for efficiently adsorbing N_2, as illustrated in Fig. 4(a). On account of the boron-decoration, the band structure of phosphorene was considerably tailored and the electrical conductance of the photocatalyst was uplifted to favour the NRR performance, as revealed in Fig. 4(b). The B-sites played a crucial role in transmitting electron-carriers from BP to N–H composites during N_2 activation.

This study provided insight into the reaction mechanism for improving the NRR activity of phosphorene due to the anchoring effect of the Boron atoms. Cheng *et al.*[113] theoretically anticipated the NRR efficiency of the B-incorporation and oxidation of black/blue phosphorene. Their study also included the lowering of the band energy due to boron atoms, which enhanced the light absorption range in the visible-IR region. The thermodynamic screening also indicated the favourable formation energy of the B-introduction into phosphorene at ambient temperature. Furthermore, it was ascertained that the oxidation of the black/blue phosphorene augmented the NRR response *via* end-on/side-on modes during the reaction mechanism.

Carbon derivatives-based photocatalysts

Carbon-based derivatives have shown enormous growth in their catalytic applicability, which is ascribed to their peculiar layered structure and advanced stability. Graphitic-carbon nitride (g-C_3N_4) has been most frequently exploited for photochemical NRR application among the different carbon derivatives, as it is cost-efficient, easy to fabricate, and possesses visible light band energy. Experimental characterization techniques indicate its adequate band positions of conduction and valence bands to fulfil the thermodynamic criteria for the reduction of N_2.[114,115] To highlight the catalytic efficiency of g-C_3N_4, Liu *et al.*[116] designed an Fe_2O_3/g-C_3N_4 photocatalytic system for NH_3 synthesis through NRR. The Z-scheme type heterojunction formation facilitated the interfacial charge transfer. Furthermore, it was ascertained that g-C_3N_4 was the reduction photocatalyst responsible for the NRR, whereas Fe_2O_3 was the oxidation photocatalyst. The higher specific surface area with mesoporous active sites favoured the extensive N_2 adsorption/activation as an optimized Fe_2O_3/g-C_3N_4 photocatalyst with an NH_3 generation rate of 47.9 mg L^{-1} h^{-1}, which was 6-fold higher than that of pristine g-C_3N_4. In order to activate the N-atom active sites in g-C_3N_4 such as edges/amino-N sites during NRR, Wang *et al.*[111] came up with a unique study in which, by anchoring B-atoms over g-C_3N_4, the N-atom active sites were stabilized *via* the development of B–N–C bonding that ultimately boosted the photochemical activity of g-C_3N_4 towards NH_3 production. The limited loading of boron into g-C_3N_4 enhanced the range of light absorption, and also impeded the recombination dynamics of photo-excited e^-–h^+ pairs. This was confirmed by the higher activity of the optimized photocatalyst for NH_3 evolution (~314 μmol g^{-1} h^{-1}), which was found to be 10-fold higher than bare g-C_3N_4, as can be seen in Fig. 4(c). Dong *et al.*[117] investigated the role of the nitrogen vacancy (N_v) in ameliorating the photochemical NRR performance of g-C_3N_4. As the shape and size of N_v was found to be identical to N-atoms of N_2 molecules, it thus promoted the adsorption and activation of the reactant N_2 during the reaction mechanism. Similar to this study, for the utilization of the carbon-vacancies (V_C), Zhang *et al.*[112] developed an ultrathin g-C_3N_4 having a higher V_C *via* thermal peeling technique that augmented the NRR efficiency. The group ascertained that the NRR activity of the carbon-based materials can be substantially increased by structural control at the atomic level and by the introduction of V_C in g-C_3N_4. A photochemical NRR activity test was performed in N_2 and Ar gases to determine the origin of the N-precursor for

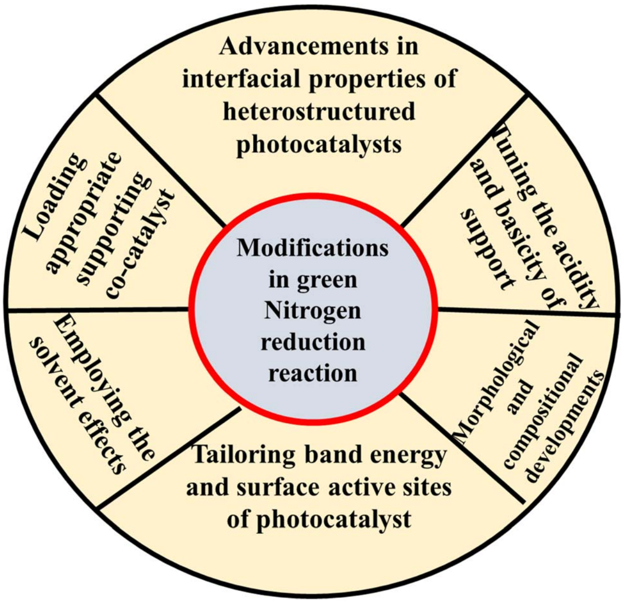

Fig. 5 Chemical strategies for advancing the photochemical NRR efficiency of catalytic systems.

Published on 27 2024. Downloaded by Fail Open on 23.07.2025 10:35:13.

N_2 fixation, as the catalyst in itself was composed of N. The control test inferred the fixed amount of NH_4^+ release in both catalytic systems, as can be seen in Fig. 4(d). The V_C-rich g-C_3N_4 showed nearly 2.25-fold higher NRR efficiency as compared to bulk-g-C_3N_4, thus manifesting the significance of V_C in augmenting the photocatalytic activity of g-C_3N_4. Other carbon-based derivatives such as graphene also exhibited a propensity to be utilized as a photocatalyst for NRR application owing to their ability to induce a higher hot electron density in the presence of visible light irradiation.[118] To support this claim, Lu *et al.*[119] demonstrated the induction of hot electrons from an Fe-decorated 3D-graphene photocatalyst to accelerate its activity and selectivity for NH_3 production at ambient conditions in the presence of a simulated light source. The as-prepared Fe@graphene photocatalyst exhibited remarkable stability without losing its activity up to 50 h. Based on the aforementioned recent advances in the photochemical NRR process *via* flatland materials, we have highlighted the strategies of ameliorating the scalability of this carbon-neutral vector in Fig. 5.

Electrochemical applications

Aiming to supplant the energy-intensive Haber–Bosch method, the electrochemical NRR to form NH_3 takes place under ambient conditions and can be propelled by renewable energy comprising solar energy, wind energy, *etc.* Thermodynamically, it has been considered that electrocatalytic NRR holds the advantage of 20% greater energy efficiency in comparison to the Haber–Bosh process.[120] However, an effective electrochemical NRR has been evinced to be exceptionally challenging due to the need of a considerable amount of energy to break the N_2 triple bond.[121] Additionally, HER is the competitive process in electrocatalytic NRR as its theoretical reductive potential is less than NRR.[122] It is widely known that one of the most crucial parameters in electrochemical NRR is the conductivity of materials; hence, the search for novel electrocatalysts to surpass the challenging issues is necessary for the electrocatalytic NRR industrial applications.[123] In general, noble metal catalysts display significant activity, but their scarcity and high cost limit their far-reaching applications. As a result, research studies have changed focus to non-noble metals-derived catalytic systems, such as carbon derivatives, MXenes, TMDs, TMPs. Electrochemical NRR is a typical heterogeneous reaction that comprises the adsorption of N_2 molecule at the catalytically active surface of the catalyst, hydrogenation and desorption of NH_3 molecule or other intermediates. According to reduction and protonation sequences and the breaking of $N\equiv N$ bonds, electrochemical NRR can be classified into dissociative and associative mechanisms. In the dissociative mechanism, the $N\equiv N$ bond is broken at the time of adsorption, resulting in the adsorption of discrete N atoms separated by a defined distance. In the successive step, hydrogenation takes place on each N atom, leading to the construction of NH_3 that is released in the last step. In the associative mechanism, the $N\equiv N$ bond stays intact after the adsorption of N_2 and breaks at the time of hydrogenation. Consequently, the associative pathway is more complex than the dissociative route, and can be further simplified according to the hydrogenation sequences into distal, alternating, and enzymatic pathways. In the distal route, the hydrogenation preferentially takes place on the N atom that is away from the catalytic surface, inclining to the adsorption of one nitrogen atom after the release of the first NH_3 on the catalytic surface. In the following steps, the successive hydrogenation of the remaining N atoms leads to the construction of a second NH_3 molecule. In the alternating route, the hydrogenation takes place on two N atoms alternatively and $N\equiv N$ bond breaks with the generation of the first NH_3 at the last step, which leaves one NH_3 molecule behind.[124] In contrast to the alternating route, N_2 adsorbs at the catalytic surface in the very first step in the enzymatic route. The subsequent steps are similar to those in the alternating route.[125] Recently, the Mars-van Krevelen mechanism was developed by Abghoui and Skulason. In this mechanism, the lattice N atoms are reduced to NH_3 on the surface of transition-metal nitrides (TMNs) and N vacancies are thus created.[126] These vacancies chemically adsorb N_2 molecules for electrochemical NRR to occur continuously. Therefore, a suitable electrocatalyst for effective NRR is rather critical that can ensure the convenient reaction mechanism in order to attain higher NH_3 efficiency.

MXenes and MBenes-based electrocatalysts

MXenes are a novel type of 2D materials possessing a high specific surface area, good electrical conductivity, stability and hydrophilic behaviours, making these flatland materials potential candidates for electrocatalytic NRR applications. Shi *et al.*[127] fabricated the N-doped-Ti_V-$Ti_{3-x}C_2T_y$-1.2 MXene for electrocatalytic NRR. The introduction of Ti vacancies improved the adsorption and activation of N_2. Furthermore, the N-dopant species enhanced the desorption of NH_3. The optimized level of the N doping content and Ti vacancy density in the as-synthesized MXene boosted the electrocatalytic NRR with the rate of 24.33 $\mu g\ h^{-1}\ mg_{cat}^{-1}$ of NH_3 and around 10% faradaic efficiency (FE) through the promotion of kinetic desorption and activation barriers of NH_3. Ba *et al.*[128] designed Ti_3AlC_2 MAX/Ti_3C_2 MXene electrocatalysts for N_2 fixation. The difference of the surface potential between MXene and MAX was around 40 mV, indicating that the electron can be easily migrated from MAX to MXene over the interfaces. This was beneficial for N_2 fixation, resulting in a remarkable FE of ∼40% and rate of 2.73 $\mu g\ h^{-1}\ cm^{-2}$ of NH_3. The outstanding NRR activity was ascribed to the unique MXene/MAX heterostructure framework that offered suitable and rich active centers to assist in the N_2 adsorption billiard sequence, hydrogenation and $N\equiv N$ bond breaking. Guo *et al.*[129] altered the surface of $Ti_3C_2T_x$ (MXene) by introducing Fe to attain high surface reactivity for the NRR. The optimized MXene/$TiFeO_x$-700 electrocatalyst exhibited remarkable performance with an NH_3 production rate of 2.19 $\mu g\ cm^{-2}\ h^{-1}$ and FE of 25.44% for the NRR. The improved catalytic activity was credited to the high surface reactivity of as-prepared optimized electrocatalyst generated through the reduction of inactive F*/OH* terminals and the rational decrement in the

Published on 27 2024. Downloaded by Fail Open on 23.07.2025 10:35:13.

surface work function, which revealed the higher number of active sites to bind N_2 and accelerated the electron migration from the catalytic surface to the intermediates of the reaction, enhancing the NRR. Du *et al.*[130] incorporated Ni nanoparticles on $V_4C_3T_x$ MXene (Ni/MX) for effective electrocatalytic N_2 fixation that performed exceptionally well by achieving ~21.3 μg h^{-1} $mg_{cat}{}^{-1}$ yield of NH_3. The enhanced performance was credited to the synergistic pathway by the O vacancy of $V_4C_3T_x$ and the Ni sites in the nanoparticles, achieving excellent enhancement of the NRR performance on the MXene based nanocomposites. Niu *et al.*[131] examined the transition metal atom-assisted $Ti_3C_2T_2$ MXene along with O/OH terminals for electrocatalytic NRR. The catalytic activity of the transition metal single atoms was investigated by their capability of adsorption on MXene, and also their potential to bind and desorb N_2 and NH_3, respectively. The OH termination in the as-synthesized electrocatalyst improved the N_2 adsorption and suppressed the adsorption of NH_3. The results displayed that $Ni/Ti_3C_2O_{0.19}(OH)_{1.81}$ showed rational kinetics and thermodynamics for electrocatalytic NRR. Another class of flatland materials having unique characteristics and structure, transition metal borides termed as MBenes have recently shown immense potential in energy-driven applications. The exotic nature of B in MBenes in terms of bonding and conductivity has led to growing research interest in these 2D materials. Zhang *et al.*[132] demonstrated FeB_2 as a novel catalytic system for electrochemical nitrate reduction into NH_3. The synergetic relationship between Fe and the B atomic-sites augmented the rate of activation of nitrate and the rate of hydrogenation of the intermediary species to achieve higher NH_3 selectivity. As high as 96.8% FE was obtained with 25.5 mg h^{-1} cm^{-2} rate of NH_3 generation at −0.6 V overpotential. Recently, Feng *et al.*[133] carried out a high-throughput screening of hexagonal-MBene electrocatalysts to determine their NRR efficiency. The authors ascertained that the catalytic response of MBenes can be tuned by bimetallic anchoring effects. It was concluded that this compositional modification leads to the regulation of the orbital energy redistribution in MBenes, and ultimately ameliorates the binding limit of the N-based intermediate species over the MBene-active sites. Gao *et al.*[134] examined the electrochemical NRR activity of hexagonal-$Zr(Hf)_2B_2O_2$ nanosheets-decorated SAC. The theoretical simulations inferred the low overpotential value of −0.10 V with higher NRR selectivity against the competitive HER process. These recent studies endorse the MXenes and MBenes tandem electrocatalysts as the state-of-art catalytic systems for efficient electrochemical NRR application.

TMDs-based electrocatalysts

TMDs have been extensively examined for a number of electrochemical reactions such as HER, oxygen reduction reaction (ORR), CO_2RR, and OER because of their tunable electronic structures to attain high catalytic performance.[135] It is quite obvious that the revealed edge defects of TMDs are the favourable active sites for HER catalysis. Therefore, decreasing edge defects can activate their capability for NRR catalysis applications. Chen *et al.*[136] fabricated a series of transition metal (TM)/WS_2 and examined their electrocatalytic performance for NRR. The results illustrated that Os/WS_2, Tc/WS_2 and Cr/WS_2 showed the best catalytic performance. The adsorbed N_2 can be efficiently transformed into NH_3 following the distal mechanism pathway together with −0.33, −0.27 and −0.37 V limiting potentials, respectively, as a consequence of the suppressed dynamics of the HER competing process. Yang *et al.*[137] synthesized hollow $MoSe_2$ nanospheres as an effective electrocatalyst for NRR. The results exhibited the rate of 11.2 μg h^{-1} $mg_{cat}{}^{-1}$ of NH_3 production and 14.2% FE that was credited to the greater number of active sites, higher surface area and the longer retention time of N_2 in the shells due to the hollow structure of the as-prepared electrocatalyst. Chu *et al.*[138] investigated the MoS_2/C_3N_4 heterostructure for electrochemical NRR *via in situ* growth of MoS_2 on C_3N_4 nanosheets utilizing the solvothermal method, as represented in Fig. 6(a). The proton nuclear magnetic resonance (^1H NMR) spectrum showed a doublet chemical shift upon providing $^{15}N_2$ gas after electrochemical NRR. A triplet chemical shift was also displayed upon providing $^{14}N_2$ gas. Meanwhile, the peaks of $^{15}NH_4{}^+$ and $^{14}NH_4{}^+$ were undetectable in Ar gas, as shown in Fig. 6(b). The current density for 2 hours at various potentials is displayed in Fig. 6(c). The as-synthesized electrocatalyst exhibited enhanced NRR activity with the yield of 18.5 μg h^{-1} mg^{-1} of NH_3 and FE of 17.8%, which was much better than that of pristine MoS_2 and C_3N_4, as illustrated in Fig. 6(d) and (e). DFT calculations showed that the interfacial charge migration from C_3N_4 to MoS_2 can improve the NRR activity of MoS_2/C_3N_4 by boosting the stability of the intermediate and simultaneously reducing the reaction energy barrier. Ling *et al.*[139] reported the WS_2/WO_2 electrocatalyst for efficient NRR that exhibited the rate of 8.53 μg_{NH3} h^{-1} $mg_{cat}{}^{-1}$ for NH_3 production with 13.5% FE, which was better than that of pristine WS_2. The enhanced activity was ascribed to the incorporation of WO_2 that efficiently suppressed the HER due to the blocking of the edge defects in WS_2 and concurrent formation of planar defects at the heterostructure as active sites for effective NRR. Liu *et al.*[140] reported an interesting study in which synergetic effects between bridged-S atoms and metallic sites over the 1T-MoS_2 phase were exploited in achieving higher electrochemical NRR performance. S-rich metallic MoS_2 yielded as high as ~99 μg h^{-1} $mg_{cat}{}^{-1}$ NH_3 with nearly 23% FE, which was found to be one of the highest among the MoS_2-based reports of NRR as of now. Theoretical studies also corroborated the favourable adsorption energy and lowered energy barrier during the reaction mechanism. The as-designed electrocatalyst also depicted the higher NH_3 selectivity and remarkable competitiveness during NRR.

TMPs and phosphorene-based electrocatalysts

Much attraction has been garnered by TMPs due to their low cost, distinct physical and chemical features, controllable components, in addition to TMPs specifically exhibiting remarkable results as electrocatalysts. Integrating phosphorus

This journal is © The Royal Society of Chemistry 2024

Published on 27 2024. Downloaded by Fail Open on 23.07.2025 10:35:13.

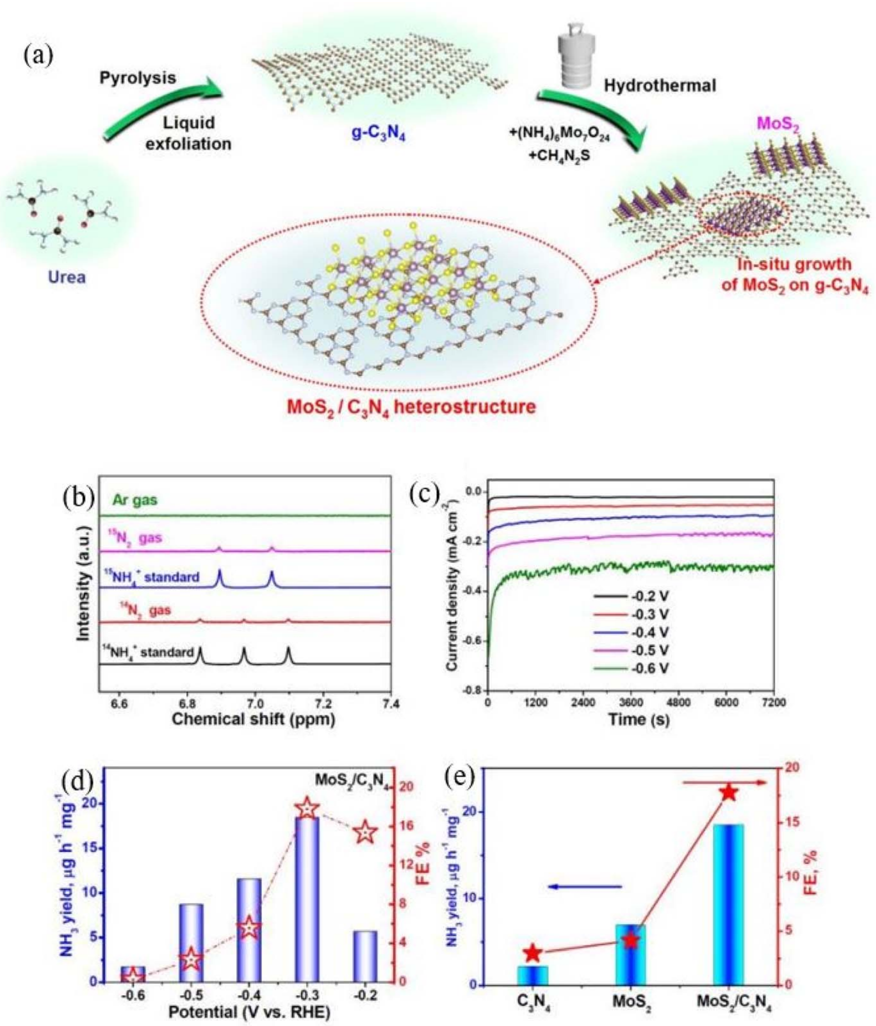

Fig. 6 (a) Schematic representation of the MoS_2/C_3N_4 heterostructure fabrication. (b) NMR depiction of MoS_2/C_3N_4. (c) Current densities of MoS_2/C_3N_4 at different potentials. (d) Yield and FEs of NH_3 at various potentials. (e) NRR activities of MoS_2, C_3N_4 and MoS_2/C_3N_4. Reproduced with permission.[138] Copyright 2020, American Chemical Society.

(P) into the transition metal lattices can alter the internal electronic structure of metals, thus enhancing the intrinsic catalytic performance. Although the utilization of TMPs in NRR has not been explored more, Rytelewska *et al.*[141] reported Fe_2P for electrochemical NRR. The as-prepared electrocatalyst showed inhibition for HER, providing around 60% FE and an NH_3 production rate of 7.5 µmol cm^{-2} h^{-1}. The improved results were attributed to the interfacially reduced iron in the presence of P network sites that activated and reduced N_2. Su *et al.*[142] designed RhP_x and a N, P-doped carbon framework as a highly efficient electrocatalyst for NRR. The catalytic behaviour and electronic structure of RhP_x were altered by tuning the P contents in the composites. DFT calculations illustrated that the incorporation of P into Rh eased the intermediate process of the catalytic reaction and reduced the catalytic reaction barrier. The results exhibited 7.64% FE and 37.6 µg h^{-1} $mg_{cat}{}^{-1}$ NH_3 production in accordance with the higher stability and selectivity possessed by the optimized electrocatalyst. Luo *et al.*[143] engineered Mo/FeP through the thermo-assisted hydrolysis method, as shown in Fig. 7(a), for the electrochemical transformation of N_2 to NH_3. The chronoamperometry results displayed steady current densities at various potentials under 2 hours electrolysis, indicating the outstanding stability (Fig. 7(b)). Also, the ultraviolet visible (UV-vis) spectra at the potential range from −0.2 V to −0.6 V is shown in Fig. 7(c). The as-synthesized nanosphere possessed remarkable catalytic activity with the rate of 13.1 µg h^{-1} mg^{-1} for $NH_4{}^+$ yield and ~7.5% FE, as illustrated in Fig. 7(d) and (e). The enhanced results stemmed from the Mo doping that was beneficial for the adsorbed N_2 molecule polarization, facilitating the easier dissociation of the N≡N bond.

Wu *et al.*[144] examined the NRR taking place on the monolayers of iron-based phosphides. The Mo-doped Fe_3P and Fe_2P monolayers effectively boosted the electrocatalytic NRR with −0.17 and −0.30 V onset potential. Additionally, the Fe and Mo atoms served as bimetallic active sites that corroborated the linear relationship at the time of the NRR pathway. Wang *et al.*[145] highlighted the anchoring effects of bimetallic Cu–Ru

Published on 27 2024. Downloaded by Fail Open on 23.07.2025 10:35:13.

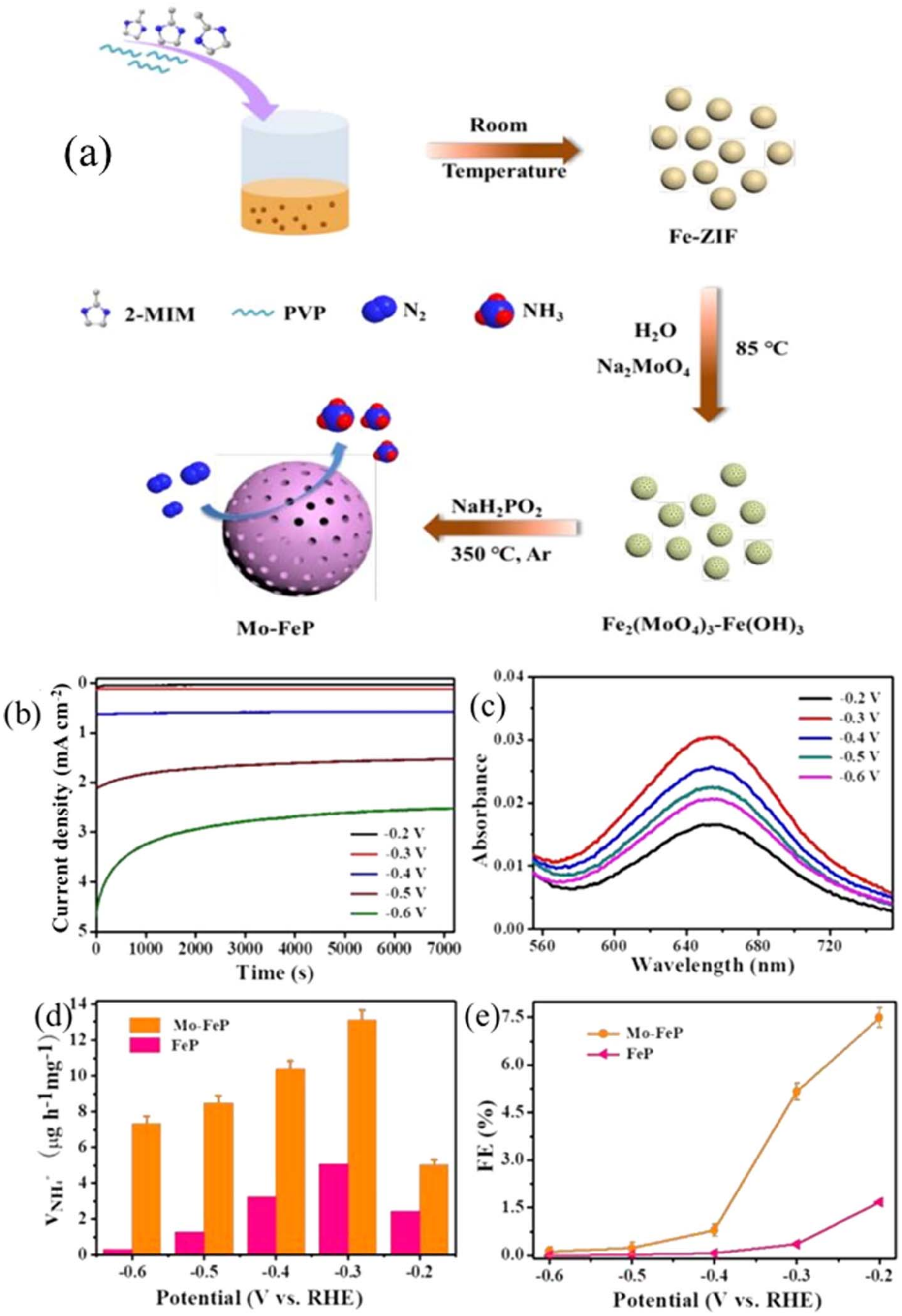

Fig. 7 (a) The synthesis method of the Mo–FeP nanosphere. (b) Current density plots of Mo–FeP at distinct applied potentials. (c) UV-vis absorption spectra tinted with the indophenol indicator for the electrolytes after electrochemical NRR from −0.2 V to −0.6 V. (d) Yield of NH_4^+ and (e) FEs of Mo–FeP and FeP at various potentials. Reproduced with permission.[143] Copyright 2020, American Chemical Society.

atoms over N-loaded phosphorene (NP) in enhancing the rate of the electrochemical NRR. The results manifested the lower overpotential value of 0.3 V of the as-designed electrocatalyst for N_2 reduction into NH_3. The electron donor–acceptor relationship of π–d electrons facilitated the activation of N_2 that is fundamental for its hydrogenation into NH_3. The symbiotic relationship between Cu–Ru and NP was further confirmed by the lowering of the NH_3-desorption energy ascribed to the higher availability of the exposed active sites.

Carbon derivatives-based electrocatalysts

At present, graphene and its derivatives have become propitious metal-free electrocatalysts possessing several distinctive features, such as tunable porosity, high surface area, outstanding stability, and conductivity and abundant defects. These merits of mass transfer and reinforcing electrons and

Published on 27 2024. Downloaded by Fail Open on 23.07.2025 10:35:13.

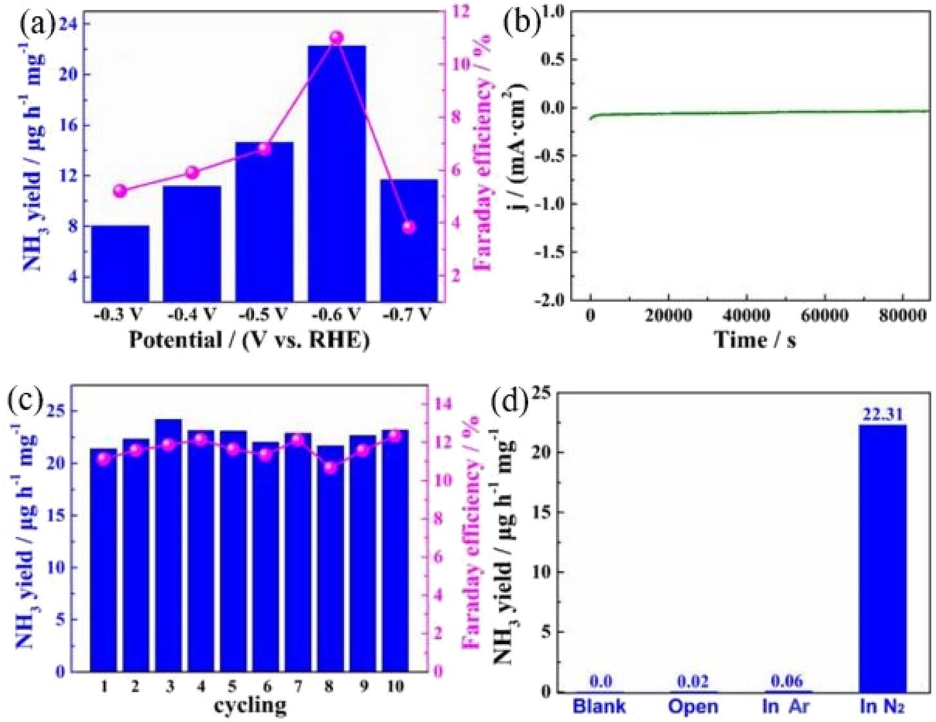

Fig. 8 (a) FEs and yield of NH_3 at distinct potentials for BHGO. (b) Current density curve of BHGO for 80 000 seconds. (c) Ten electrocatalytic cycles at −0.6 V for BHGO. (d) Yield of NH_3 of blank and after 2 hours electrolysis at different conditions. Reproduced with permission.[146] Copyright 2020, Elsevier.

higher active sites offer efficient NRR. Wang *et al.*[146] synthesized broken holey graphene oxide (BHGO) for electrocatalytic NRR, and compared the activity of the optimized electrocatalyst with holey graphene oxide (HGO) and graphene oxide (GO). The BHGO displayed higher active sites and greater electron migration capability. Therefore, it showed outstanding NRR activity and stability with an NH_3 yield of 22.27 μg h^{-1} mg^{-1} and ~11% FE at ambient conditions, as shown in Fig. 8(a) and (b). Also, the yield and FE of NH_3 almost remained constant for 10 cycles, as displayed in Fig. 8(c). The source of the N element had also been examined by carrying out the experiment in blank and control environments. The results demonstrated that there was no NH_3 detected except for when N_2 was used as the feed gas, as shown in Fig. 8(d). Moreover, DFT simulations showed that the insertion of multi-dimensional coordinated defects improved the adsorption of N_2, decreased the energy barrier at the rate-determining step, and profoundly redistributed the charge. Zhang *et al.*[147] designed reduced graphene oxide (rGO) consisting of tuned defects for NRR. The as-synthesized rGO having defect sites (including unsaturated carbon) displayed enhanced NH_3 selectivity because of the robust binding of N_2 in place of the H^+ ions. The as-prepared dopant-free electrocatalyst showed the FE as high as 22% and an NH_3 production yield of ~7.5 μg h^{-1} mg^{-1}. Liu *et al.*[148] fabricated a MoS_2/rGO electrocatalyst for N_2 fixation. The homogeneous distribution of MoS_2 on rGO and the C–S–C linking bonds among them benefitted the electrocatalyst and offered abundant active sites, boosting the electron migration in the reaction that galvanized an outstanding FE of ~28% and nearly 16.5 μg h^{-1} $mg_{cat}{}^{-1}$ yield of NH_3. Moreover, the as-prepared electrocatalyst displayed high electrochemical stability and selectivity.

Wang *et al.*[149] synthesized an Fe_3O_4/rGO electrocatalyst for NRR having remarkable stability, selectivity and activity, with an achieved NH_3 rate of ~28 μg h^{-1} mg^{-1} and FE of ~19% at ambient conditions. The enhanced NRR activity stemmed from the chemical coupling impact between the Fe_3O_4 particles and rGO that resulted in the improvement of the binding affinity of N_2 molecules, decreasing the free energy of the reaction and notably ameliorating the conductivity. Wang *et al.*[150] engineered In_2O_3/rGO, and determined the experimental and theoretical evidences to support the remarkable NRR activity of the heterostructured electrocatalyst. DFT studies manifested that the exposed facets of In_2O_3 favoured the efficient N_2 adsorption, which ultimately led to the improved cleaving of N–N bonds and following hydrogenation steps during NRR. This ultimately restricted the HER kinetics and resulted in a lower NRR overpotential. Therefore, the as-synthesized electrocatalyst showed excellent NRR activity with ~8% FE and the rate of NH_3 yield was found to be 18.4 μg h^{-1} mg^{-1}.

Techno-economic assessment of NRR

It is known that nearly 50% of the H_2 evolved globally is consumed as one of the primary reactant feeds of the NH_3 preparation process *via* Haber–Bosch technique. Therefore, sustainable NH_3 production holds great significance, which is

Published on 27 2024. Downloaded by Fail Open on 23.07.2025 10:35:13.

very much achievable due to the lowering prices of renewable electricity across the globe and because of the abundant solar energy.[151] For the determination of the economic viability of the NH_3 synthesis *via* NRR process, techno-economic analysis (TEA) is an important indicator that encompasses the various segments of the proposed technology and its market size globally. It is a methodology that can be employed to estimate the economic feasibility of NRR, as it combines the engineering principles with economic analysis to assess the cost of green NH_3 fuel, benefits, and risks associated with it.[151–154] To obtain the balanced equilibrium between the cost and production of NH_3, the photochemical and electrochemical NRR should be more efficient than the conventional Haber–Bosch process for its industrial competitiveness. As of now, the production cost of the latter technology is estimated to be nearly 600 dollars per ton by comprising different costs of transporting and storing NH_3.[155,156] Pozo *et al.*[157] evaluated the viability of green NH_3 production as a carbon-neutral energy vector. The group carried out cash flow investigations, which inferred that based on the gas-switching reforming, a levelized cost of $\sim$332 € per ton is achievable as compared to traditional NH_3 production plants ($\sim$385.5 € per ton). Pawar *et al.*[154] examined the TEA of NH_3 generation by employing renewable resources of wind, solar and electrical energies. The group revealed that India can achieve the higher NH_3 efficiency with cost as low as 723 and 765 EUR per t_{NH_3} towards national and international usage. Progress in TEA of green NH_3 will play a vital role in channelizing the NRR technology to a scalable platform. However, TEA alongside life-cycle assessments (LCA) have certain disadvantages which limit their effectiveness in providing a complete scenario of green NH_3 generation refinery, such as resource intensiveness, limited scope of analysis, and assumption sensitivity. Nevertheless, TEA remains a valuable technique for providing detailed insights into the economic viability and risks of NH_3 production *via* NRR. It is essential to recognize and address these limitations to ensure that the TEA results are robust, reliable, and actionable.

Conclusions

Photochemical and electrochemical NRR have emerged as potential alternative pathways of the energy-exhaustive conventional Haber–Bosch (HB) route to produce NH_3 efficiently at lower cost. The generation of green NH_3 alongside HER and CO_2RR is the environmentally benign energy carrier that promises to achieve a carbon-neutral society. Herein, we have discussed photochemical and electrochemical NRR applications in light of the ever-evolving flatland materials by taking into consideration their remarkable physicochemical properties. Recent advances in 2D-materials-utilized photochemical NRR operations have been described with the main preference given to those materials which have achieved decent progress in green NH_3 synthesis in the past few years, such as MXenes and MBenes, TMDs, TMPs, carbon derivatives and phosphorene. In addition, the electrochemical NRR applications of 2D materials have been summarized to highlight their experimental achievements in achieving higher faradaic efficiency and NH_3 selectivity. Different types of reports have been discussed to bolster the catalytic design of flatland materials for efficient photochemical and electrochemical NRR performance. The catalytic efficiency of flatland materials can be augmented by engineering unique heterostructured catalysts and introducing surface defects to improve the optoelectronic and surface properties in order to ameliorate the charge-transfer dynamics and electrical conductance of 2D materials. Techno-economic assessment of NH_3 has also been surveyed to indicate the current status of NRR, and where this technology stands as the contender of a sustainable energy resource.

Future outlook

Photochemical and electrochemical pathways of NRR offer promising perspectives for sustainable NH_3 synthesis, providing opportunities to address environmental challenges and transition towards a greener and more energy-efficient nitrogen fixation process. Here, we have aimed to discuss the most important factors that should be taken into consideration for an efficient NRR process *via* flatland materials-based catalytic systems, as shown in Fig. 9.

(1) As compared to the exploitation of 2D materials in other energy conversion applications of HER and CO_2RR, the literature of NRR is still in its nascent stage. This is attributed to several contributing factors, such as the complexity of the reaction mechanism, low yield, sluggish dynamics, and its lower thermodynamic feasibility as compared to the competitive HER process.[158–160]

Nevertheless, various chemical strategies are in the developing phase for impeding the rate of the competitive HER during nitrogen fixation, such as: (1) designing catalysts with tailored surface properties and active sites that selectively

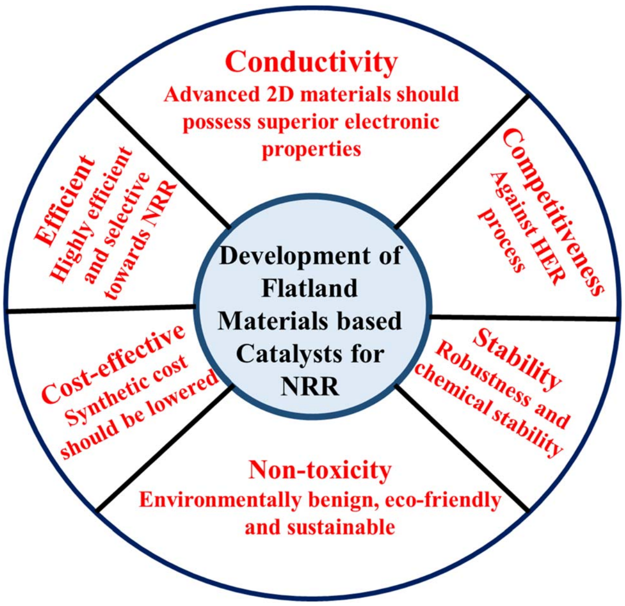

Fig. 9 Significant variables to enhance the effectiveness of flatland materials-based catalytic systems for NRR.

This journal is © The Royal Society of Chemistry 2024

Published on 27 2024. Downloaded by Fail Open on 23.07.2025 10:35:13.

promote the NRR over the HER by providing favourable free energies for N_2 capture in contrast to the H^+-adsorption. In this quest, Liao *et al.*[95] provided the superior chemisorption of N_2 over H-atoms during photochemical NRR process, as also discussed in aforementioned reports. Furthermore, engineering flatland materials with controlled surface morphology/hierarchical structure are the other prospects of ameliorating the NRR efficiency. (2) Decoration of exposed facets of 2D-materials can also lead to the modification of their electronic properties, thus assisting in improving the selectivity towards NRR. For instance, the incorporation of metallic/non-metallic dopants (as highlighted by Wang *et al.*[108]) by utilizing Co-dopant in Ni_2P nanosheets. (3) Surface modification of 2D materials in such fashion that functionalizes their catalytic surface with ligands/functional groups for preferential binding of N_2 molecules and facilitates their activation and reduction, such as introduction of heteroatoms (N, P, B) into the catalyst. For instance, Wang *et al.*[110] ascertained the anchoring effects of B-atoms in augmenting the N_2 adsorption ability of P-phosphorene on account of exploiting vacant and filled sp^2- and p-orbitals during the NRR process. In a similar manner, Dong *et al.*[117] examined the role of the nitrogen vacancy (N_v) in improving the N_2 capture ability of g-C_3N_4 by exploiting the identical geometry of N_v and N-atoms. This report uncovered an excellent surface engineering strategy to augment the NRR activity by enhancing the N_2 binding. (4) Optimization of the operational reaction conditions (such as temperature, pressure, pH, electrolyte composition) and utilization of sacrificial electron donor species to improve the NRR performance over its HER counterpart. Moreover, in electrochemical processes, the applied potential can be equilibrated to shift the reaction dynamics towards NRR, while minimizing the rate of HER. For instance, utilization of electrolytes with high ionic conductivity and low HER overpotential can suppress the HER and enhance the NRR. (5) Hampering the HER-active sites by introducing inhibitors that selectively block or deactivate sites on the catalyst surface is another strategy of promoting the rate of NRR. This can be achieved by employing strategies that can passivate or modify specific exposed sites on the surface of flatland materials that otherwise are favourable for HER activity. For instance, the edge sites of TMDs are naturally inclined towards the adsorption of H^+ ions, ascribed to their favourable free energies. Therefore, modifying these edge sites in such fashion that NRR active sites are exposed can lead to an efficient NRR process. These are some of the most significant chemical strategies that can mitigate the rate of the competitive HER process during NRR, and enhance the selectivity and efficiency of the NH_3 production.

(2) Another important factor that governs the NRR efficiency is the stability of the catalyst and separation of NH_3 from the side reactions that take place simultaneously during the photo/electro fixing of N_2 through reductive pathways. As of now, the catalytic activity of the flatland materials is limited towards NRR with stability up to hardly hundreds of hours only. Based on this, the scalable applicability of these 2D materials is still far away and requires the addressing of factors that restrict their activity, such as robustness, recyclability during NRR, separation of NH_3 and its oxidation into nitrite/nitrate species *via* activated O-radicals.[161]

(3) To fully optimize the catalytic performance of flatland materials, a comprehension of the mechanistic sketch is requisite during photochemical and electrochemical NRR applications. Owing to the complex reaction mechanism of NRR, machine learning tools and theoretical modelling should be employed to investigate the surface-active sites that involve favourable free energies for N_2 adsorption/activation. The role of non-covalent interactions, chemical modifications and chemical environment effects during surface reactions should be extensively scrutinized using different experimental techniques to determine the kinetics of intermediates that are formed during the reaction mechanism of N_2 fixation.[3] Existing computational models are able to ascertain the formation energies of different intermediates. However, the anticipations of theoretical data should be confirmed *via* experimental tools. Therefore, researchers should focus on developing theoretical-experimental problems to accelerate the pace of NH_3 formation *via* NRR process.[10] The state-of-art atomic-level characterization and *in situ* techniques can play a crucial role in obtaining scalability in NH_3 synthesis.

(4) One of the most significant approaches of enhancing the quantum efficiency during NRR operations is the fabrication of catalytic systems that exhibit an ideal band structure with visible light-driven band energy, as the driving potential involved in N_2 reduction is 1.17 V. However, the role of other half-oxidation reactions should not be undermined as the produced NH_3 is prone to the oxidation reaction. For identifying the reactions that take place at the valence band of the photocatalyst, high-throughput screening of HER can be utilized, which has been discussed in detail in reviews elsewhere.[162]

Data availability

No primary research results, software or code have been included, and no new data were generated or analysed as part of this review.

Conflicts of interest

The authors declare no financial competing interest.

Acknowledgements

T. A. thanks the SERB sponsored research scheme (CRG/2023/000480) and UGC, Govt. of India for Research Grants for In-service Faculty Members for financial support. S. A. A. and I. S. acknowledge UGC for research fellowships.

References

1 S. A. Ali and T. Ahmad, *Mater. Today Chem.*, 2023, **29**, 101387.

2 S. C. Peter, *ACS Energy Lett.*, 2018, **3**, 1557–1561.

3 S. A. Ali, I. Sadiq and T. Ahmad, *Mater. Today Sustain.*, 2023, **24**, 100587.

Published on 27 2024. Downloaded by Fail Open on 23.07.2025 10:35:13.

4 J. Fu, K. Jiang, X. Qiu, J. Yu and M. Liu, *Mater. Today*, 2020, **32**, 222–243.
5 A. Mehtab, S. A. Ali, I. Sadiq, S. Shaheen, H. Khan, M. Fazil, N. A. Pandit, F. Naaz and T. Ahmad, *ACS Sustainable Resour. Manage.*, 2024, **1**(4), 604–620.
6 A. Mehtab and T. Ahmad, *ACS Catal.*, 2024, **14**, 691–702.
7 Z. Huang, M. Rafiq, A. R. Woldu, Q. X. Tong, D. Astruc and L. Hu, *Coord. Chem. Rev.*, 2023, **478**, 214981.
8 S. A. Ali and T. Ahmad, *Inorg. Chem.*, 2024, **63**, 304–315.
9 H. Liu, J. Timoshenko, L. Bai, Q. Li, M. Rüscher, C. Sun, B. R. Cuenya and J. Luo, *ACS Catal.*, 2023, **13**, 1513–1521.
10 G. Zhang, Y. Li, C. He, X. Ren, P. Zhang and H. Mi, *Adv. Energy Mater.*, 2021, **11**, 2003294.
11 J. Lim, C. A. Fernández, S. W. Lee and M. C. Hatzell, *ACS Energy Lett.*, 2021, **6**, 3676–3685.
12 F. Rehman, S. Kwon, M. D. Hossain, C. B. Musgrave III, W. A. Goddard III and Z. Luo, *J. Mater. Chem. A*, 2022, **10**, 23323–23331.
13 J. Hou, M. Yang and J. Zhang, *Nanoscale*, 2020, **12**, 6900–6920.
14 O. A. Ojelade, S. F. Zaman and B. J. Ni, *J. Environ. Manage.*, 2023, **342**, 118348.
15 L. Kang, W. Pan, J. Zhang, W. Wang and C. Tang, *Fuel*, 2023, **332**, 126150.
16 B. Sun, S. Lu, Y. Qian, X. Zhang and J. Tian, *Carbon Energy*, 2023, **5**, e305.
17 H. Song, D. A. C. Haro, P. W. Huang, L. Barrera and M. C. Hatzell, *Acc. Chem. Res.*, 2023, **56**, 2944–2953.
18 D. Hao, Y. Liu, S. Gao, H. Arandiyan, X. Bai, Q. Kong, W. Wei, P. K. Shen and B. J. Ni, *Mater. Today*, 2021, **46**, 212–233.
19 Y. Kong, X. Li, A. R. P. Santiago and T. He, *J. Am. Chem. Soc.*, 2024, **146**, 5987–5997.
20 G. Ren, J. Zhao, Z. Zhao, Z. Li, L. Wang, Z. Zhang, C. Li and X. Meng, *Angew. Chem., Int. Ed.*, 2024, **63**, e202314408.
21 X. Wei, C. Chen, X. Z. Fuand and S. Wang, *Adv. Energy Mater.*, 2024, **14**, 2303027.
22 H. Khan, S. E. Lofland, J. Ahmed, K. V. Ramanujachary and T. Ahmad, *Int. J. Hydrogen Energy*, 2024, **58**, 717–725.
23 U. Farooq and T. Ahmad, *Int. J. Hydrogen Energy*, 2024, **64**, 290–300.
24 Y. He, M. Wang, L. Zhang, Q. Cheng, S. Liu, X. Sun, Y. Jiang, T. Qian and C. Yan, *Adv. Funct. Mater.*, 2024, 2315548.
25 Y. Xiong, B. Li, Y. Gu, T. Yan, Z. Ni, S. Li, J. L. Zuo, J. Ma and Z. Jin, *Nat. Chem.*, 2023, **15**, 286–293.
26 S. A. Ali, S. Majumdar, P. K. Chowdhury, N. Alhokbany and T. Ahmad, *ACS Appl. Energy Mater.*, 2024, **7**, 2881–2895.
27 S. Shaheen, S. A. Ali, U. F. Mir, I. Sadiq and T. Ahmad, *Catalysts*, 2023, **13**, 1046.
28 S. A. Ali and T. Ahmad, *Int. J. Hydrogen Energy*, 2023, **48**, 22044–22059.
29 A. L. Marinho, C. Comminges, A. Habrioux, S. Célérier, N. Bion and C. Morais, *Chem. Commun.*, 2023, **59**, 10133–10136.
30 Y. Ruan, Z. H. He, Z. T. Liu, W. Wang, L. Hao, L. Xu, A. Robertson and Z. Sun, *J. Mater. Chem. A*, 2023, **11**, 22590–22607.
31 N. Sathishkumar and H. T. Chen, *ACS Appl. Mater. Interfaces*, 2023, **15**, 15545–15560.
32 Y. Pang, C. Su, L. Xu and Z. Shao, *Prog. Mater. Sci.*, 2023, **132**, 101044.
33 M. Arif, G. Yasin, L. Luo, W. Ye, M. A. Mushtaq, X. Fang, X. Xiang, S. Ji and D. Yan, *Appl. Catal., B*, 2020, **265**, 118559.
34 F. Du, J. Yao, H. Luo, Y. Chen, Y. Qin, Y. Du, Y. Wang, W. Hou, M. Shuai and C. Guo, *Green Chem.*, 2024, **26**, 895–903.
35 A. Mehtab, S. A. Ali, P. P. Ingole, Y. Mao, S. M. Alshehri and T. Ahmad, *ACS Appl. Energy Mater.*, 2023, **6**, 12003–12012.
36 P. Y. Chen, M. Liu, Z. Wang, R. H. Hurt and I. Y. Wong, *Adv. Mater.*, 2017, **29**, 1605096.
37 Z. Dai, L. Liu and Z. Zhang, *Adv. Mater.*, 2019, **31**, 1805417.
38 M. C. Lemme, D. Akinwande, C. Huyghebaert and C. Stampfer, *Nat. Commun.*, 2022, **13**, 1392.
39 H. Tao, Q. Fan, T. Ma, S. Liu, H. Gysling, J. Texter, F. Guo and Z. Sun, *Prog. Mater. Sci.*, 2020, **111**, 100637.
40 F. R. Fan, R. Wang, H. Zhang and W. Wu, *Chem. Soc. Rev.*, 2021, **50**, 10983–11031.
41 N. Rohaizad, C. C. Mayorga-Martinez, M. Fojtů, N. M. Latiff and M. Pumera, *Chem. Soc. Rev.*, 2021, **50**, 619–657.
42 H. Wang, J. Chen, Y. Lin, X. Wang, J. Li, Y. Li, L. Gao, L. Zhang, D. Chao, X. Xiao and J. M. Lee, *Adv. Mater.*, 2021, **33**, 2008422.
43 X. Hui, X. Ge, R. Zhao, Z. Li and L. Yin, *Adv. Funct. Mater.*, 2020, **30**, 2005190.
44 C. Feng, Z. P. Wu, K. W. Huang, J. Ye and H. Zhang, *Adv. Mater.*, 2022, **34**, 2200180.
45 G. Swain, S. Sultana and K. Parida, *Nanoscale*, 2021, **13**, 9908–9944.
46 Y. Meng, J. Feng, S. Han, Z. Xu, W. Mao, T. Zhang, J. S. Kim, I. Roh, Y. Zhao, D. H. Kim and Y. Yang, *Nat. Rev. Mater.*, 2023, **8**, 498–517.
47 I. Sadiq, S. Asim Ali and T. Ahmad, *Catalysts*, 2023, **13**, 109.
48 M. Zhao, C. Casiraghi and K. Parvez, *Chem. Soc. Rev.*, 2024, **53**, 3036–3064.
49 P. D. Pedersen, T. Vegge, T. Bligaard and H. A. Hansen, *ACS Catal.*, 2023, **13**, 2341–2350.
50 H. Jin, L. Li, X. Liu, C. Tang, W. Xu, S. Chen, L. Song, Y. Zheng and S. Z. Qiao, *Adv. Mater.*, 2019, **31**, 1902709.
51 W. Y. Chen, S. N. Lai, C. C. Yen, X. Jiang, D. Peroulis and L. A. Stanciu, *ACS Nano*, 2020, **14**, 11490–11501.
52 J. Zou, J. Wu, Y. Wang, F. Deng, J. Jiang, Y. Zhang, S. Liu, N. Li, H. Zhang, J. Yu and T. Zhai, *Chem. Soc. Rev.*, 2022, **51**, 2972–2990.
53 S. A. Ali, I. Sadiq and T. Ahmad, *Langmuir*, 2024, **40**, 10414–10432.
54 Y. Liu, Y. H. Li, X. Li, Q. Zhang, H. Yu, X. Peng and F. Peng, *ACS Nano*, 2020, **14**, 14181–14189.
55 T. Ahmad, G. Kavitha, C. Narayana and A. K. Ganguli, *J. Mater. Res.*, 2005, **20**, 1415–1421.
56 T. Ahmad and A. K. Ganguli, *J. Am. Ceram. Soc.*, 2006, **89**, 1326–1332.
57 T. Ahmad, M. Shahazad, M. Ubaidullah, J. Ahmed, A. Khan and A. M. El-Toni, *Mater. Res. Express*, 2017, **4**, 125016.

This journal is © The Royal Society of Chemistry 2024

Published on 27 2024. Downloaded by Fail Open on 23.07.2025 10:35:13.

58 M. Fazil, S. M. Alshehri, Y. Mao and T. Ahmad, *Catalysts*, 2023, **13**(5), 893.
59 T. Ahmad, S. Khatoon, K. Coolahan and S. E. Lofland, *J. Alloys Compd.*, 2013, **558**, 117–124.
60 R. Phul, C. Kaur, U. Farooq and T. Ahmad, *Mater. Sci. Eng. Int. J.*, 2018, **2**(4), 90–94.
61 M. S. Javed, X. Zhang, T. Ahmad, M. Usman, S. S. A. Shah, A. Ahmad, I. Hussain, S. Majeed, M. R. Khawar, D. Choi and C. Xia, *Mater. Today*, 2024, **74**, 121–148.
62 K. R. G. Lim, M. Shekhirev, B. C. Wyatt, B. Anasori, Y. Gogotsi and Z. W. Seh, *Nat. Synth.*, 2022, **1**, 601–614.
63 N. Miao, Y. Gong, H. Zhang, Q. Shen, R. Yang, J. Zhou, H. Hosono and J. Wang, *Angew. Chem.*, 2023, **135**, e202308436.
64 O. Mashtalir, M. Naguib, V. N. Mochalin, Y. Dall'Agnese, M. Heon, M. W. Barsoum and Y. Gogotsi, *Nat. Commun.*, 2013, **4**, 1716.
65 D. Wang, C. Zhou, A. S. Filatov, W. Cho, F. Lagunas, M. Wang, S. Vaikuntanathan, C. Liu, R. F. Klie and D. V. Talapin, *Science*, 2023, **379**, 1242–1247.
66 F. Han, S. Luo, L. Xie, J. Zhu, W. Wei, X. Chen, F. Liu, W. Chen, J. Zhao, L. Dong and K. Yu, *ACS Appl. Mater. Interfaces*, 2019, **11**, 8443–8452.
67 C. Wang, H. Shou, S. Chen, S. Wei, Y. Lin, P. Zhang, Z. Liu, K. Zhu, X. Guo, X. Wu and P. M. Ajayan, *Adv. Mater.*, 2021, **33**, 2101015.
68 T. Najam, S. S. A. Shah, L. Peng, M. S. Javed, M. Imran, M. Q. Zhao and P. Tsiakaras, *Coord. Chem. Rev.*, 2022, **454**, 214339.
69 E. T. Akgul, O. C. Altıncı, A. Umay, P. Aghamohammadi, A. A. Farghaly, P. Ma, Y. Chen and M. Demir, *J. Energy Storage*, 2024, **84**, 110882.
70 S. A. Ali and T. Ahmad, *Int. J. Hydrogen Energy*, 2022, **47**, 29255–29283.
71 Z. Liu, S. Yang, B. Sun, X. Chang, J. Zheng and X. Li, *Angew Chem., Int. Ed.*, 2018, **57**, 10187–10191.
72 L. Xiong, B. Wang, H. Cai, H. Hao, J. Li, T. Yang and S. Yang, *Appl. Catal., B*, 2021, **295**, 120283.
73 A. Mehtab, Y. Mao, S. M. Alshehri and T. Ahmad, *J. Colloid Interface Sci.*, 2023, **652**, 1467–1480.
74 N. Mounet, M. Gibertini, P. Schwaller, D. Campi, A. Merkys, A. Marrazzo, T. Sohier, I. E. Castelli, A. Cepellotti, G. Pizzi and N. Marzari, *Nat. Nanotechnol.*, 2018, **13**, 246–252.
75 S. H. Choi, S. J. Yun, Y. S. Won, C. S. Oh, S. M. Kim, K. K. Kim and Y. H. Lee, *Nat. Commun.*, 2022, **13**, 1484.
76 T. M. Boland and A. K. Singh, *Comput. Mater. Sci.*, 2022, **207**, 111238.
77 S. Milana, *Nat. Nanotechnol.*, 2019, **14**, 919–921.
78 H. Jin, S. S. Kim, S. Venkateshalu, J. Lee, K. Lee and K. Jin, *Adv. Sci.*, 2023, **10**, 2300951.
79 T. T. Liu, D. D. Zhai, B. T. Guan and Z. J. Shi, *Chem. Soc. Rev.*, 2022, **51**, 3846–3861.
80 X. Chen, Y. Guo, X. Du, Y. Zeng, J. Chu, C. Gong, J. Huang, C. Fan, X. Wang and J. Xiong, *Adv. Energy Mater.*, 2020, **10**, 1903172.
81 B. Yang, W. Ding, H. Zhang and S. Zhang, *Energy Environ. Sci.*, 2021, **14**, 672–687.
82 N. Morlanés, S. P. Katikaneni, S. N. Paglieri, A. Harale, B. Solami, S. M. Sarathy and J. Gascon, *Chem. Eng. J.*, 2021, **408**, 127310.
83 C. Kurien and M. Mittal, *Int. J. Hydrogen Energy*, 2023, **48**, 28803–28823.
84 S. Sun, Q. Jiang, D. Zhao, T. Cao, H. Sha, C. Zhang, H. Song and Z. Da, *Renewable Sustainable Energy Rev.*, 2022, **169**, 112918.
85 D. Ye and S. C. E. Tsang, *Nat. Synth.*, 2023, **2**, 612–623.
86 Y. Wei, W. Jiang, Y. Liu, X. Bai, D. Hao and B. J. Ni, *Nanoscale*, 2022, **14**, 2990–2997.
87 Y. Pang, C. Su, G. Jia, L. Xu and Z. Shao, *Chem. Soc. Rev.*, 2021, **50**, 12744–12787.
88 A. N. Singh, R. Anand, M. Zafari, M. Ha and K. S. Kim, *Adv. Energy Mater.*, 2024, 2304106.
89 M. Ozkan, K. A. Quiros, J. M. Watkins, T. M. Nelson, N. D. Singh, M. Chowdhury, T. Namboodiri, K. R. Talluri and E. Yuan, *Chem*, 2024, **10**, 443–483.
90 R. Zhao, Y. Chen, H. Xiang, Y. Guan, C. Yang, Q. Zhang, Y. Li, Y. Cong and X. Li, *ACS Appl. Mater. Interfaces*, 2023, **15**, 6797–6806.
91 Y. Ruan, Z. H. He, Z. T. Liu, W. Wang, L. Hao, L. Xu, A. Robertson and Z. Sun, *J. Mater. Chem. A*, 2023, **11**, 22590–22607.
92 S. A. Ali and T. Ahmad, *Langmuir*, 2024, **40**, 10835–10846.
93 W. Gao, X. Li, S. Luo, Z. Luo, X. Zhang, R. Huang and M. Luo, *J. Colloid Interface Sci.*, 2021, **585**, 20–29.
94 C. Hao, Y. Liao, Y. Wu, Y. An, J. Lin, Z. Gu, M. Jiang, S. Hu and X. Wang, *J. Phys. Chem. Solids*, 2020, **136**, 109141.
95 Y. Liao, J. Qian, G. Xie, Q. Han, W. Dang, Y. Wang, L. Lv, S. Zhao, L. Luo, W. Zhang and H. Y. Jiang, *Appl. Catal., B*, 2020, **273**, 119054.
96 Z. Shen, F. Li, L. Guo, X. Zhang, Y. Wang, Y. Wang, X. Jian, X. Gao, Z. Wang, R. Li and C. Fan, *Appl. Catal., B*, 2024, **346**, 123732.
97 Q. Zhang, Q. Li, H. Li, X. Shi, Y. Zhou, Q. Ye, R. Yang, D. Li and D. Jiang, *Inorg. Chem.*, 2023, **62**, 12138–12147.
98 H. Guo, H. Zhang, J. Zhao, P. Yuan, Y. Li, Y. Zhang, L. Li, S. Wang and R. Song, *J. Phys. Chem. C*, 2022, **126**, 3043–3053.
99 Z. Li, N. H. Attanayake, J. L. Blackburn and E. M. Miller, *Energy Environ. Sci.*, 2021, **14**, 6242–6286.
100 T. Ma, R. Li, Y. C. Huang, Y. Lu, L. Guo, M. Niu, X. Huang, R. A. Soomro, J. Ren, Q. Wang and B. Xu, *ACS Catal.*, 2024, **14**, 6292–6304.
101 B. Hu, B. H. Wang, Z. J. Bai, L. Chen, J. K. Guo, S. Shen, T. L. Xie, C. T. Au, L. L. Jiang and S. F. Yin, *Chem. Eng. J.*, 2022, **442**, 136211.
102 L. Yao, Y. Yu, X. Xu, Z. Du, T. Yang, J. Hu and H. Huang, *J. Colloid Interface Sci.*, 2024, **654**, 189–200.
103 L. Ye, C. Han, Z. Ma, Y. Leng, J. Li, X. Ji, D. Bi, H. Xie and Z. Huang, *Chem. Eng. J.*, 2017, **307**, 311–318.
104 J. Qin, W. Zhao, X. Hu, J. Li, P. Ndokoye and B. Liu, *ACS Appl. Mater. Interfaces*, 2021, **13**, 7127–7134.
105 K. Sun, M. Liu, J. Pei, D. Li, C. Ding, K. Wu and H. L. Jiang, *Angew. Chem.*, 2020, **132**, 22937–22943.

Published on 27 2024. Downloaded by Fail Open on 23.07.2025 10:35:13.

106 Y. Shi, M. Li, Y. Yu and B. Zhang, *Energy Environ. Sci.*, 2020, **13**, 4564–4582.

107 X. Gao, B. Zhang, L. Cao, F. Liu, H. Fan, C. Wang and J. Xu, *J. Environ. Chem. Eng.*, 2024, **12**, 112276.

108 Z. Wang, L. Xu, X. Yin, Y. Liu, Y. Chen, Q. Wang and W. Yang, *Int. J. Hydrogen Energy*, 2024, **51**, 809–819.

109 S. Rana, A. Kumar, P. Dhiman, G. Sharma, J. Amirian and F. J. Stadler, *Fuel*, 2024, **356**, 129630.

110 M. Wang, Z. Xu, X. Zhang, J. Yang, J. Liu, G. Qiao and G. Liu, *Appl. Surf. Sci.*, 2021, **554**, 149614.

111 W. Wang, H. Zhou, Y. Liu, S. Zhang, Y. Zhang, G. Wang, H. Zhang and H. Zhao, *Small*, 2020, **16**, 1906880.

112 Y. Zhang, J. Di, P. Ding, J. Zhao, K. Gu, X. Chen, C. Yan, S. Yin, J. Xia and H. Li, *J. Colloid Interface Sci.*, 2019, **553**, 530–539.

113 Y. Cheng, Y. Song and Y. Zhang, *Phys. Chem. Chem. Phys.*, 2019, **21**, 24449–24457.

114 M. Majumder, H. Saini, I. Dedek, A. Schneemann, N. R. Chodankar, V. Ramarao, M. S. Santosh, A. K. Nanjundan, S. Kment, D. Dubal and M. Otyepka, *ACS Nano*, 2021, **15**, 17275–17298.

115 W. J. Ong, L. L. Tan, Y. H. Ng, S. T. Yong and S. P. Chai, *Chem. Rev.*, 2016, **116**, 7159–7329.

116 S. Liu, S. Wang, Y. Jiang, Z. Zhao, G. Jiang and Z. Sun, *Chem. Eng. J.*, 2019, **373**, 572–579.

117 G. Dong, W. Ho and C. Wang, *J. Mater. Chem. A*, 2015, **3**, 23435–23441.

118 D. Brida, A. Tomadin, C. Manzoni, Y. J. Kim, A. Lombardo, S. Milana, R. R. Nair, K. S. Novoselov, A. C. Ferrari, G. Cerullo and M. Polini, *Nat. Commun.*, 2013, **4**, 1–9.

119 Y. Lu, Y. Yang, T. Zhang, Z. Ge, H. Chang, P. Xiao, Y. Xie, L. Hua, Q. Li, H. Li and B. Ma, *ACS Nano*, 2016, **10**, 10507–10515.

120 S. L. Foster, S. I. P. Bakovic, R. D. Duda, S. Maheshwari, R. D. Milton, S. D. Minteer, M. J. Janik, J. N. Renner and L. F. Greenlee, *Nat. Catal.*, 2018, **1**, 490.

121 X. Chen, Y. Guo, X. Du, Y. Zeng, J. Chu, C. Gong, J. Huang, C. Fan, X. Wang and J. Xiong, *Adv. Energy Mater.*, 2019, **10**, 1903172.

122 J. H. Montoya, C. Tsai, A. Vojvodic and J. K. Nørskov, *ChemSusChem*, 2015, **8**, 2180.

123 Y. Huang, D. D. Babu, Z. Peng and Y. Wang, *Adv. Sci.*, 2020, **7**, 1902390.

124 Y. Wang, W. Zhou, R. Jia, Y. Yu and B. Zhang, *Angew Chem., Int. Ed.*, 2020, **59**, 5350.

125 K. C. MacLeod and P. L. Holland, *Nat. Chem.*, 2013, **5**, 559.

126 P. Mars and D. W. van Krevelen, *Chem. Eng. Sci.*, 1954, **3**, 41.

127 Y. Shi and Y. Liu, *Appl. Catal., B*, 2021, **297**, 120482.

128 K. Ba, D. Pu, X. Yang, T. Ye, J. Chen, X. Wang, T. Xiao, T. Duan, Y. Sun, B. Ge and P. Zhang, *Appl. Catal., B*, 2022, **317**, 121755.

129 Y. Guo, T. Wang, Q. Yang, X. Li, H. Li, Y. Wang, T. Jiao, Z. Huang, B. Dong, W. Zhang and J. Fan, *ACS Nano*, 2020, **14**, 9089–9097.

130 C. F. Du, L. Yang, K. Tang, W. Fang, X. Zhao, Q. Liang, X. Liu, H. Yu, W. Qi and Q. Yan, *Mater. Chem. Front.*, 2021, **5**, 2338–2346.

131 K. Niu, L. Chi, J. Rosen and J. Bjork, *J. Phys. Chem. Lett.*, 2022, **13**, 2800–2807.

132 G. Zhang, X. Li, K. Chen, Y. Guo, D. Ma and K. Chu, *Angew. Chem., Int. Ed.*, 2023, **62**, e202300054.

133 S. Feng, Y. Yao, J. C. Charlier, G. M. Rignanese and J. Wang, *Chem. Mater.*, 2023, **35**, 9019–9028.

134 Y. Gao, E. Wang, Y. Zheng, J. Zhou and Z. Sun, *Energy Mater. Adv.*, 2023, **4**, 0039.

135 C. R. Zhu, D. Gao, J. Ding, D. Chao and J. Wang, *Chem. Soc. Rev.*, 2018, **47**, 4332–4356.

136 Y. Chen, X. Zhang, J. Qin and R. Liu, *Appl. Surf. Sci.*, 2022, **571**, 151357.

137 L. Yang, H. Wang, X. Wang, W. Luo, C. Wu, C. A. Wang and C. Xu, *Inorg. Chem.*, 2020, **59**, 12941–12946.

138 K. Chu, Y. P. Liu, Y. B. Li, Y. L. Guo and Y. Tian, *ACS Appl. Mater. Interfaces*, 2020, **12**, 7081–7090.

139 Y. Ling, F. M. Kazim, S. Ma, Q. Zhang, K. Qu, Y. Wang, S. Xiao, W. Cai and Z. Yang, *J. Mater. Chem. A*, 2020, **8**, 12996–13003.

140 R. Liu, H. Fei, J. Wang, T. Guo, F. Liu, Z. Wu and D. Wang, *Appl. Catal., B*, 2024, **343**, 123469.

141 B. Rytelewska, A. Chmielnicka, T. Chouki, M. Skunik-Nuckowska, S. Naghdi, D. Eder, A. Michalowska, T. Ratajczyk, E. Pavlica, S. Emin and Y. Fu, *Electrochim. Acta*, 2023, **471**, 143360.

142 J. Su, H. Zhao, W. Fu, W. Tian, X. Yang and H. Z. Y. Wang, *Appl. Catal., B*, 2020, **265**, 118589.

143 Y. X. Luo, W. B. Qiu, R. P. Liang, X. H. Xia and J. D. Qiu, *ACS Appl. Mater. Interfaces*, 2020, **12**, 17452–17458.

144 J. Wu, J. H. Li and Y. X. Yu, *Catal. Sci. Technol.*, 2021, **11**, 1419–1429.

145 M. Wang, R. Song, Q. Zhang, C. Li, Z. Xu, G. Liu, N. Wan and S. Lei, *Fuel*, 2022, **321**, 124101.

146 F. Wang, H. Wang and J. Mao, *Colloids Surf., A*, 2020, **605**, 125345.

147 M. Zhang, C. Choi, R. Huo, G. H. Gu, S. Hong, C. Yan, S. Xu, A. W. Robertson, J. Qiu, Y. Jung and Z. Sun, *Nano Energy*, 2020, **68**, 104323.

148 Y. Liu, W. Wang, S. Zhang, W. Li, G. Wang, Y. Zhang, M. Han and H. Zhang, *ACS Sustain. Chem. Eng.*, 2020, **8**, 2320–2326.

149 F. Wang, L. Xia, X. Li, W. Yang, Y. Zhao and J. Mao, *Energy Environ. Mater.*, 2021, **4**, 88–94.

150 P. Wang, Q. Q. Li, Y. H. Cheng and K. Chu, *J. Mater. Sci.*, 2020, **55**, 4624–4632.

151 L. Wang, M. Xia, H. Wang, K. Huang, C. Qian, C. T. Maravelias and G. A. Ozin, *Joule*, 2018, **2**, 1055–1074.

152 J. R. Gomez, J. Baca and F. Garzon, *Int. J. Hydrogen Energy*, 2020, **45**, 721–737.

153 O. Osman, S. Sgouridis and A. Sleptchenko, *J. Cleaner Prod.*, 2020, **271**, 121627.

154 N. D. Pawar, H. U. Heinrichs, C. Winkler, P. M. Heuser, S. D. Ryberg, M. Robinius and D. Stolten, *Int. J. Hydrogen Energy*, 2021, **46**, 27247–27267.

155 B. M. Comer, P. Fuentes, C. O. Dimkpa, Y. H. Liu, C. A. Fernandez, P. Arora, M. Realff, U. Singh, M. C. Hatzell and A. J. Medford, *Joule*, 2019, **3**, 1578–1605.

This journal is © The Royal Society of Chemistry 2024

156 G. Hochman, A. S. Goldman, F. A. Felder, J. M. Mayer, A. J. Miller, P. L. Holland, L. A. Goldman, P. Manocha, Z. Song and S. Aleti, *ACS Sustain. Chem. Eng.*, 2020, **8**, 8938–8948.

157 C. A. Del Pozo and S. Cloete, *Energy Convers. Manage.*, 2022, **255**, 115312.

158 X. Zhao, G. Hu, G. F. Chen, H. Zhang, S. Zhang and H. Wang, *Adv. Mater.*, 2021, **33**, 2007650.

159 C. Ling, Y. Zhang, Q. Li, X. Bai, L. Shi and J. Wang, *J. Am. Chem. Soc.*, 2019, **141**, 18264–18270.

160 Y. Ren, C. Yu, X. Tan, H. Huang, Q. Wei and J. Qiu, *Energy Environ. Sci.*, 2021, **14**, 1176–1193.

161 H. Hirakawa, M. Hashimoto, Y. Shiraishi and T. Hirai, *ACS Catal.*, 2017, **7**, 3713–3720.

162 M. Umer, S. Umer, M. Zafari, M. Ha, R. Anand, A. Hajibabaei, A. Abbas, G. Lee and K. S. Kim, *J. Mater. Chem. A*, 2022, **10**, 6679–6689.

Published on 27 2024. Downloaded by Fail Open on 23.07.2025 10:35:13.